Fluid or flop? Investigating the metasomatism at North Doherty pluton.

Abby Brodsky

Advisor: Dr. Penniston-Dorland

11/29/2021

GEOL394

Table of Contents

1. Abstract

Skarns are a vital part of economic geology; skarns can host ores such as Fe, Au, W, and Mo; these elements are needed for everyday electronics. The granodiorite North Doherty pluton in southwest Montana is emplaced in limestone, and in places around the pluton exotic skarn minerals formed. The skarn appearance around the pluton is discontinuous and is interrupted by marble and recrystallized limestone. Due to the irregular distribution of the skarn around the pluton, questions arise such as “Why did the skarn develop in some areas and not others? What elements are gained or lost due to metasomatism? And “What is the source and composition of the skarn-forming fluids?". To evaluate these questions, eight samples were collected, seven are from along a traverse away from the pluton, four skarn, and two limestone, one pluton granodiorite sample, and one sample from another smaller skarn roof pendant in the pluton were studied. The six carbonate samples from the traverse were then investigated using x-ray fluorescence (XRF), petrography, electron probe microanalyzer (EPMA), Raman spectroscopy, and mass spectrometry. Bulk-rock XRF data was collected from the samples and was compared to determine changes in composition, showing no major systematic variation of the bulk chemistry when compared to distance. However significant % mass loss of Rb, Ba, K, Sr, and Pb was shown. Petrography was used to determine the minerals present and interpret changes in mineralogy along the transect associated with bulk chemistry variations. The petrography data indicates complex mineralogy with minerals such as vesuvianite, wollastonite, scawtite chrysotile, lizardite, phlogopite, pyrite, andradite-schorlomite-grossular, grossular-andradite and calcite. Observations suggest that chrysotile, lizardite, some calcite, and scawtite formed during retrogression. The electron probe microanalyzer (EPMA) was used to determine mineral chemistry and to confirm mineral identities. The Raman spectrometer was used to further identify mineral identities that were not confirmed from the EPMA, identifying chrysotile, lizardite, andradite-schorlomite-grossular, and scawtite. The mass spectrometer was used to study the oxygen and carbon isotopes in the calcite to indicate if metasomatic fluids derived from the pluton played a role in the development of the mineralogy of the rocks. Using the geochemical and petrography data collected, petrologic calculations were performed using bulk XRF data in Perple_X to constrain the fluid composition and was unsuccessful. The calculations indicate a water-rich fluid of X_{CO2} <0.27. The stable isotope analysis indicates that it is likely that both devolatilization and fluid derived from the pluton altered the isotopic composition of the skarn rocks. The research provides insight into the fluid composition coming from the pluton and the chemical changes caused by interaction of the pluton with the limestone.

2. Introduction

Skarn deposits are an important part of economic geology. Skarns can form in a multitude of environments, and most commonly around plutons (Meinert et al., 2005). When a pluton is emplaced into limestone in the presence of fluids, it can produce skarns. The ores concentrated in the skarns are critical for the economy. The elements in skarns include, tungsten, iron, copper, zinc, lead, gold, rare earth elements (REEs), and tin (Meinert, 1992). These are needed for many everyday appliances such as cellphones and cars. In fact, skarn deposits are the world's largest

source for tungsten (Meinert et al., 2005). The skarn ore deposits around plutons tend to vary in age and are as young as late Tertiary and as old as Precambrian (Einaudi and Burt, 1982; Meinert, 1992).

Located in southwest Montana the intermediate North Doherty pluton has a discontinuous outcropping of skarn around its margins. This skarn is not economically viable due to a lack of ore-bearing minerals. However, understanding the role of fluid in skarn formation, how the fluid movement and composition altered and changed the country rock, can give insight why other plutons are economically viable. The study of North Doherty pluton will help contribute to the understanding of how skarns form, and how fluid composition plays a role in mineral formation. Additionally, North Doherty skarn has exotic minerals forming that have not been well studied. Understanding the role of fluid in skarn formation, how the fluid movement and composition altered and changed the country rock, can give insight why other plutons are economically viable.

This research evaluates the origin and composition of the fluid that caused the skarn. Understanding how fluid moves through skarns can help predict where an economically viable skarn may form. For this to be completed, non-economically skarns need to be studied in addition to the economically viable ones to differentiate in the models being made. To address these questions petrography, XRF bulk-rock analysis, mass spectrometry, EPMA, and Raman spectroscopy were conducted on the samples collected from the traverse.

A major factor in the formation of skarns is fluid chemistry which causes metasomatism and this can concentrate ores. The fluid can transport ore elements and can be either sourced from the pluton or country rock. To better understand the ore formation occurring in skarns, determining fluid sources from both unmineralized and mineralized settings is needed. The study of the unmineralized North Doherty pluton addresses these hypotheses:

1. The skarn samples have interacted with water-rich fluids.
   H_0: The skarn samples have not interacted with water rich fluids.
2. The fluid that interacted from the skarn samples has been derived from the pluton.
   H_0: The fluid that interacted from the skarn samples was derived elsewhere.

3. Geologic Background

3.1 Terminology, and definitions of skarns

Skarns are calc-silicate rock, in which distinctive calc-silicate minerals form by a change in chemistry (metasomatism), meaning fluid interacted with the rock and caused mineralogical changes. Contact metamorphism of carbonates does not always guarantee a skarn, hornfels or marble can form as well. Skarns and hornfels are distinguished from each other by geologic settings, morphology, grain size, and composition. Most skarns display metasomatic zoning (Einaudi and Burt, 1982). Depending on the protolith, skarns can further be classified as an endoskarn or exoskarn. Endoskarns refer to skarns with an igneous or pelitic protolith, while exoskarns refer to skarns with a carbonate protolith (Einaudi and Burt, 1982; Meinert, 1992).

When the protolith is not known the determination of an endoskarn vs. exoskarn is typically determined using the mineralogy present (Meinert, 1992). In the case of the skarn at North Doherty pluton, it is an exoskarn as it has a limestone protolith. Skarns can form during regional and contact metamorphism (Meinert et al., 2005). The most common metamorphic environment skarns are found next to plutons. However, skarns have also been documented to be found in areas such as by shallow geothermal systems and by major fault and shear zones (Meinert et al., 2005). The term skarn deposits are referred only to skarns with a dominant economic metal present (Einaudi and Burt, 1982). North Doherty pluton's skarn is not a skarn deposit based on this definition given.

3.2 North Doherty pluton geologic background

The granodiorite North Doherty pluton is located in southwest Montana. Within 50 miles of the pluton are two porphyry deposits: the Berkeley pit copper mine in Butte and the Golden Sunlight mine gold mine in Cardwell (Figure 1). The North Doherty pluton has a variable composition with seven different rock types present: metagabbro, gabbro, hornblende-biotite latite, basalt, monzonite, diorite, and granodiorite. The most prevalent rock type of the pluton is diorite. The pluton is emplaced into the Mississippian Lodgepole limestone and Three Forks formation (Bean, 1981). The Three Forks formation consists of calcareous siltstone and sandstone (Bean, 1981). The pluton is not chemically related to the Boulder batholith or Tobacco Root batholith; however, it does seem to be related to the regional timing of the plutonism involved in the creation of both batholiths (Bean, 1981). Bean (1981) also suggests that the North Doherty pluton may be related to the Elkhorn Mountain Volcanic system based on mineral chemistry of one sub-rock type at the pluton. The age of North Doherty is not known but is thought to be anywhere from 76 to 68 million years old, based on the ages of the nearby Tobacco Root and the Boulder batholiths (Bean, 1981). The pluton is small, less than 2 kilometers across in diameter. The depth and temperature emplacement of the pluton was determined based on the analysis of feldspars in the granodiorite. The pluton crystallized at a temperature around 950° C and the intrusion was no deeper than 1.5 kilometers (Fenn, 1968). The skarn is not continuous around the contact aureole, and much of the aureole is recrystallized limestone and marble. This indicates that in some areas there may not have been any fluid movement, the amount of fluid was small, or there was not enough time for the fluid to react with the country rock. This could be due to the variations in the magma contacting the country rock as the skarn only outcrops around the pluton next to the diorite and granodiorite.

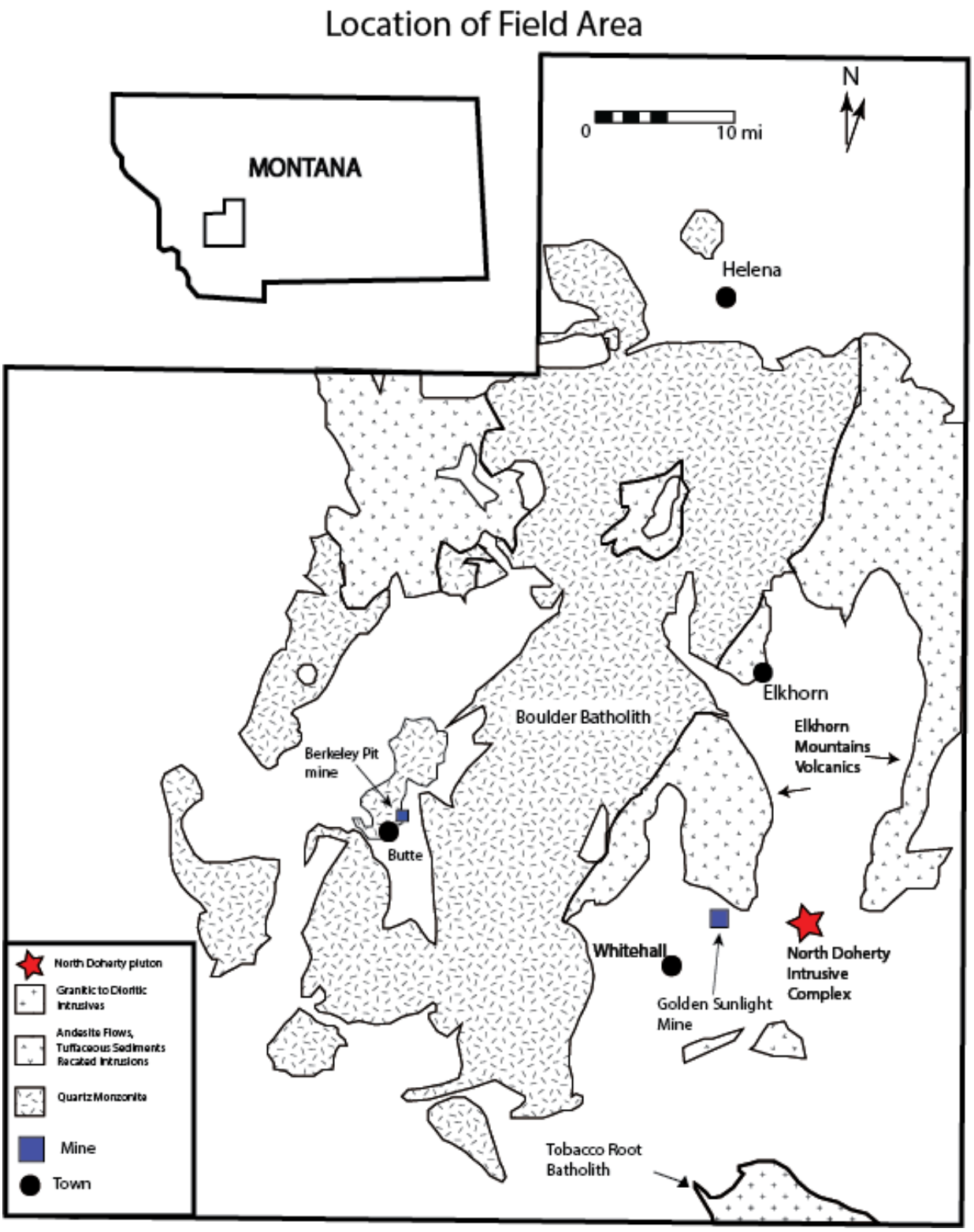

Figure 1. General geologic map of the batholiths near North Doherty pluton, modified from (Bean, 1981). Information about the lithology of the Elkhorn Mountain Volcanics, and the Boulder batholith from (Berger et al., 2011). Information on the Tobacco batholith is from (Brady et al., 2004).

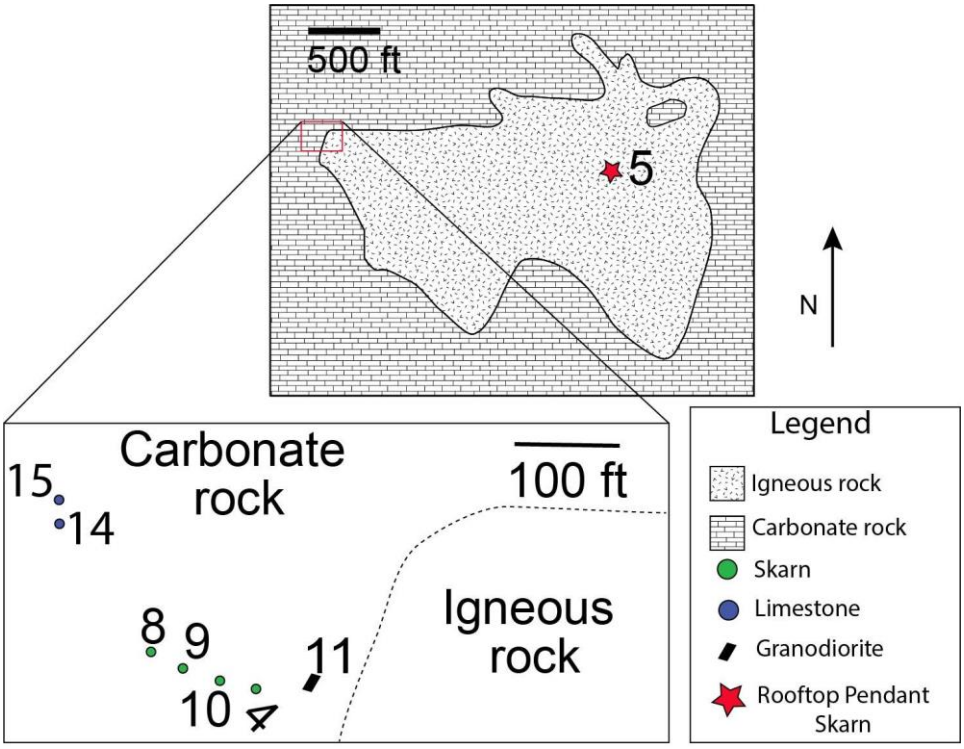

Figure 2. Map of the North Doherty pluton noting where the skarn samples were collected.

4. Methods

4.1 Samples and petrography

Seven samples were collected along a traverse starting at the pluton contact and moving outward perpendicularly from the boundary. An additional skarn sample was collected is from another outcrop, a roof pendant found in the interior of the pluton (sample 5, Figure 2). The samples had thin sections made by Wagner Petrographics Inc and, hand sample descriptions were made (See appendix I for the descriptions and hand sample photos). The samples on the map studied are 5, 4, 10, 9, 8, 14, 15, and 11 (Figure 2). The thin sections were analyzed with a Nikon Eclipse LV100 Polarizing microscope with a QImaging Micropublisher 5.0-RTV camera in the Microscope Lab at the University of Maryland. The camera was used to take plane-polarized light (PPL), cross-polarized light (XPL), and reflected light (RL) photomicrographs. The microscope was used to make preliminary determinations of minerals present in the rocks. Maps of specific thin section regions were made for use during electron probe analysis and the Raman spectrometer analysis. The modal abundances of minerals were estimated visually using the petrographic microscope.

4.2 Electron probe microanalysis

The University of Maryland's JEOL 8900R Electron Probe Microanalyzer was used under the direction of Dr. Philip Piccoli to analyze the minerals. The EPMA was used to confirm mineral identities. This was performed by collecting data from Energy-Dispersive Spectroscopy (EDS), Wavelength-Dispersive Spectroscopy (WDS), and by obtaining backscatter electron (BSE) images. EDS was used to provide qualitative chemical information and used to aid in mineral identification. WDS was used to quantitatively determine mineral chemistry, and the information was used to calculate mineral formulae. BSE images gave textural information between the different minerals. The operating conditions for EDS, WDS, and BSE imaging were 15 kV accelerating voltage and a 20 nA cup current.

4.3 Geochemical analysis

The six carbonate-bearing samples from the traverse were pulverized into a fine powder using a steel mortar and pestle, followed by an alumina ceramic shatterbox. The fine rock powders were then sent out to Franklin and Marshall College to be analyzed by their PANalytical 2404 X-ray fluorescence vacuum spectrometer. The samples were analyzed for loss of ignition, major elements, and trace-element compositions. The uncertainty on major-element composition analyzed using XRF was determined through repeat analysis of the basalt standard BHVO-2. All major elements had less than 0.5 wt.% uncertainty within two standard deviation of uncertainty CaO, Na_2O and TiO_2 had less than 0.1 wt.% of uncertainty within two standard deviations and MnO, K_2O and P_2O_5 had less than 0.01 wt.% uncertainty within 2 standard deviations of uncertainty. For accuracy on the major elements and trace elements from Franklin and Marshall College see appendices II, III, and for XRF data of the samples see appendix IV.

4.4 Stable isotope analysis

The six powdered calcite-bearing samples from the traverse were analyzed for $\delta^{18}O$ and $\delta^{13}C$. This was completed using the Isoprime mass spectrometer at the UMD stable isotope laboratory under the direction of Dr. Mike Evans.

Using standard notation, $\delta H(‰) = (\frac{(H/L)_{sample} - (H/L)_{Standard}}{(H/L)_{standard}}) * 1000$, where H is the heavier isotope, and L is the lighter isotope. The reference ratio used for reporting is ^{18}O to ^{16}O, and the standard is Vienna standard mean ocean water (VSMOW). The reference ratio for reporting is ^{13}C to ^{12}C, and the standard is Pee Dee Belemnite (VPDB). The samples were weighed out differently depending on their percent carbonate (see appendix V for sample masses weighed). The weighed samples were then sealed into exetainer vials and then loaded into a Multiflow autosampler rack that was kept at $65^{O}C$. The samples were then flushed with He and dissolved in phosphoric acid and were left to react for one hour. The CO_2 produced by the reaction between the acid and the rock sample was then passed through a Nafion water trap prior to mass analysis on an Isoprime mass spectrometer (see Evans et al., 2016 for more details).

Standards JTB and MCC were run during the analytical sessions (See appendix VI for measured standard compositions). Standard precisions are less than 0.04 ‰ for $\delta^{13}C$ and less than 0.08 ‰ for $\delta^{18}O$. The unknown isotope composition of the skarn samples was measured

three or four times depending on how much powder there was available. The variability of the measurements was less than 0.33 ‰ ($\delta^{13}C$) and 0.21 ‰ ($\delta^{18}O$) (see appendix V).

The raw sample isotope data are analyzed for within-analysis isotopic drift, runtime drift, and amplitude corrections (see Evans et al., 2016 for more details). The demonstrated median bias of the two-point correction algorithm used in Evans et al. (2016) is based on analysis of international working standard carbonate materials and is not different from zero. The precision of this analysis is better than 0.1 ‰ (Evans et al., 2016).

4.5 Perple_X

Perple_X is a suite of Fortran77 programs created by James Connolly (2009). These programs can produce a wide range of thermodynamic models. Bulk XRF data from all four skarn samples was converted into moles and used as input into Perple_X to produce T-XCO_2 and P-T pseudosections using vertex. Additionally, the T-XCO_2 conditions were calculated using reaction stoichiometry with Perple_X. The Holland and Powell (1998) database was used for the calculations as it had a wide variety of skarn minerals in it. Then based on the EPMA data collected, phase solution models for garnet, and biotite were added from White et al. (2014) to the corresponding XRF data for which each thin section relates to.

4.6 Raman spectroscopy

The Carnegie Institute of Science's Raman spectrometer was used by Dr. Andrew Steele to identify minerals that could not be further identified via mineral chemistry from the electron probe. Raman spectra were collected using WITec alpha-Scanning Near-Field Optical Microscope customized to incorporate confocal Raman spectroscopic imaging. The excitation source is a frequency-doubled solid state YAG laser with a 532 nm wavelength. Spectra were produced using integration times of 3 seconds per accumulation for 10 accumulations.

5. Results

5.1 Thin section petrography, EPMA, and Raman results

The major minerals in the skarn that are found in all the thin sections are vesuvianite, and calcite (Table 1). There are also other minerals present as well such as, calcite, chrysotile, lizardite, grossular-andradite, pyrite, wollastonite, phlogopite and monticellite. There are several exotic minerals found in thin sections as well, such as andradite-schorlomite-grossular garnets, and scawtite. Some of the minerals have different textures and colors than expected. For example, the wollastonite features simple twinning and, in some cases, a fibrous texture. The vesuvianite in all thin sections features concentric zoning, and sometimes has serpentine and calcite inclusions in the vesuvianite. In three of the skarn thin sections, vesuvianite exhibits anomalous tan and dark blue colors, a trait interpreted to be due to the presence of titanium in its mineral structure (Ahmed-Said and Leake, 1996).

Minerals present in each thin section.

	Skarn					Limestone		Pluton
	Sample 8	Sample 9	Sample 10	Sample 4	Sample 5	Sample 14	Sample 15	Sample 11
Wollastonite (Wo)		10%	25%	15%				
Vesuvianite (Ves)	15%	20%	25%	25%	10%			
Calcite (Cal)	84%	65%	35%	14%	1%	49%	59%	<1%
Grossular-andradite (Grt)		1%						
Pyrite (Py)	1%	1%	1%			2%	2%	
Muscovite						5%	<1%	
Phlogopite (Phl)		2%						
Scawtite (Sca)			2%	20%				
Andradite-schorlomite-grossular (Grt)			2%					
Chrysotile and lizardite (Srp)		1%	10%	26%				
Monticellite (Mont)					89%			
Quartz						10%	5%	10%
Clay minerals						60%	46%	
Epidote					<1%			3%
Feldspars								80%
Magnetite								1%
Titanite								2%

Table 1. Table of minerals present in each sample. These are visual approximations based on the thin section petrography. All mineral abbreviations retrieved from (Whitney & Evans, 2010).

Granodiorite petrography

The granodiorite sample contains the minerals K-feldspar, plagioclase, microcline, quartz, titanite, tourmaline, epidote, magnetite, and apatite. The feldspars tend to exhibit zoning and show evidence of alteration. These minerals were identified using the petrographic microscope.

Limestone petrography

The limestones are predominantly calcite, quartz, and some small muscovite grains along with clay minerals. The patches of the clay minerals are no bigger than 0.3mm in length, the calcite grains are no bigger than 0.2mm in length, quartz grains are no bigger 0.1mm in length and muscovite grains are no bigger than 0.15mm in length.

Skarn petrography

Vesuvianite

Vesuvianite is known to be considerably variable in its mineral composition (Deer et al., 1997). As the distance increases from the pluton, the vesuvianite progressively gets smaller.

With distance increasing the anomalous blue and tan colors of the vesuvianite disappearing to 1st order grey to black, and the concentric zoning is no longer visible (Figure 3). Another trend occurring is the Fe/Mg ratio also increases as the distance from the pluton increases. This trend is not reflected in the bulk-rock XRF Fe-Mg trends in the bulk XRF very little variation (Figure 4). The vesuvianite crystals sizes can vary to be larger than 4 mm in length and as small as 0.5mm.

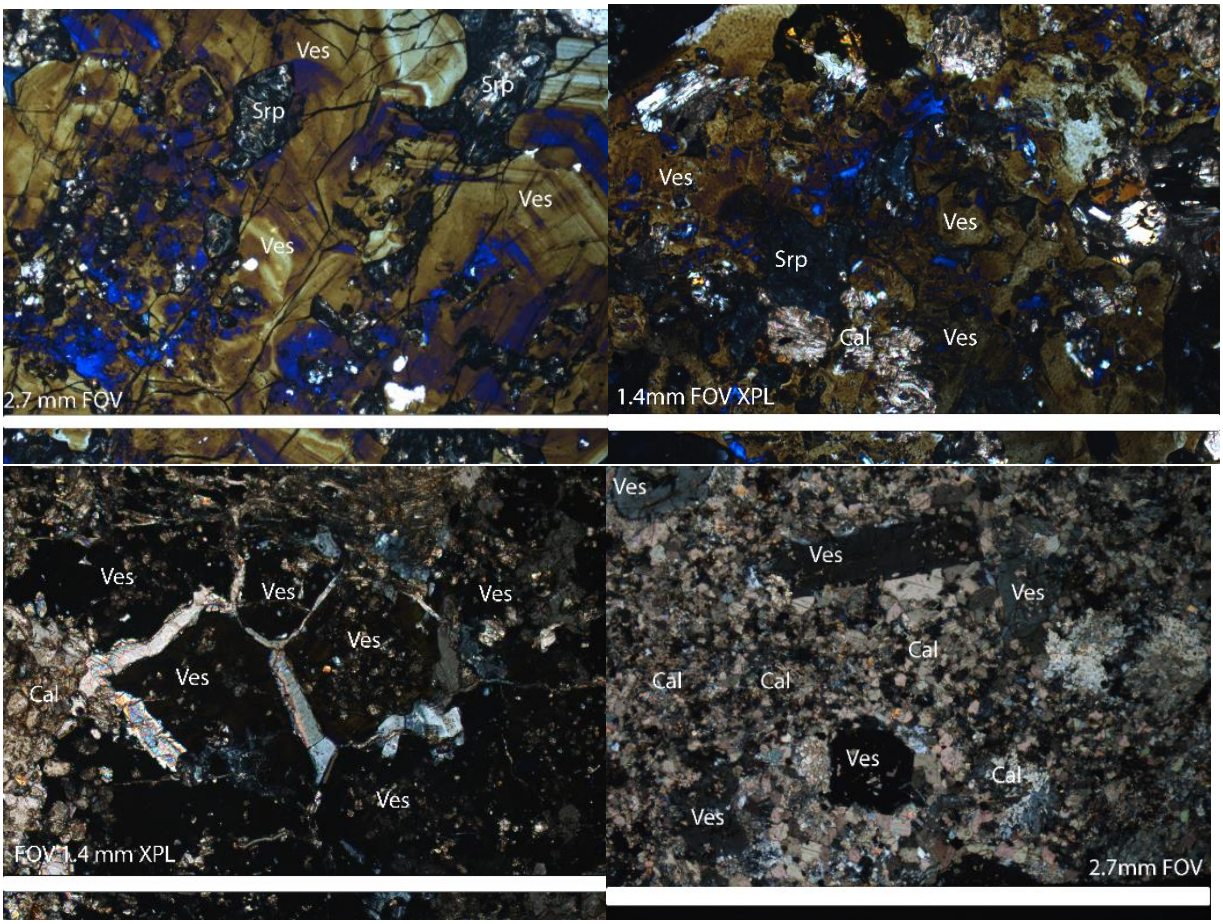

Figure 3. Photomicrographs of the vesuvianite from: sample 4 (top left, 15 meters from the pluton), sample 10 (top right, 21.7 meters from the pluton). sample 9 (bottom left, 28.3 meters from the pluton), and sample 8 (bottom right, 38.3 meters from the pluton). All photos are in XPL.

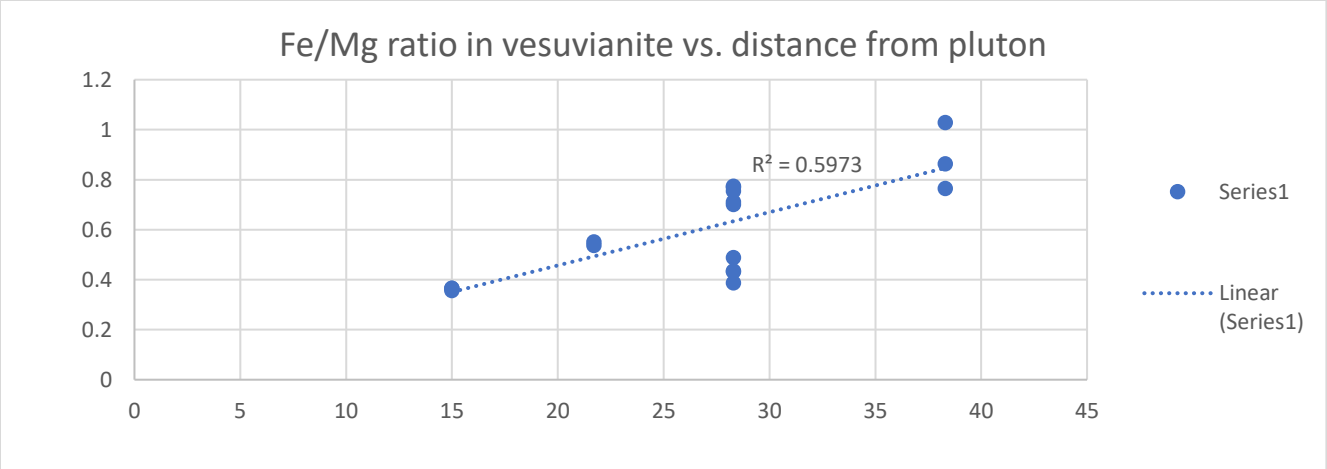

Figure 4. Plot of Fe/Mg ratio vs. distance from pluton. Sample 4 is 15 meters away, sample 10 is 21.7 meters, sample 9 is 28.3 meters, and sample 8 is 38.3 meters away from the pluton.

Vesuvianite mineral formulae (average) from WDS Analyses

Sample	Formula
Sample 4	$Ca_{18.9}Mg_{2.8}\ Al_{9.8}Fe_{1.0}\ Si_{18}O_{69}(OH)_9$
Sample 10	$Ca_{18.2}Ti_{0.4}Mg_{2.6}\ Al_{9.1}Fe_{1.4}\ Si_{18.2}O_{69}(OH)_9$
Sample 9	$Ca_{18.7}Ti_{0.3}Mg_{2.7}\ Al_{9.4}Fe_{1.5}\ Si_{18.0}O_{69}(OH)_9$
Sample 8	$Ca_{18.7}Ti_{0.6(}Mg_{1.5}\ Fe_{0.5})\ Al_{9.1}Fe_{0.9}\ Si_{18.0}O_{69}(OH)_9$

Calcite

The calcite close to the pluton varies in grain size (Figure 5); they are large euhedral grains present in sample 4 and sample 10 close to the pluton but are not present in the matrix. In sample 9 and 8 furthest from the pluton the calcite makes up the matrix around some of the larger vesuvianite grains and other minerals. The calcite is pure $CaCO_3$ in every tested thin section where EPMA analyses were done (see appendices VIII for WDS analyses and VIIII for EDS spectra).

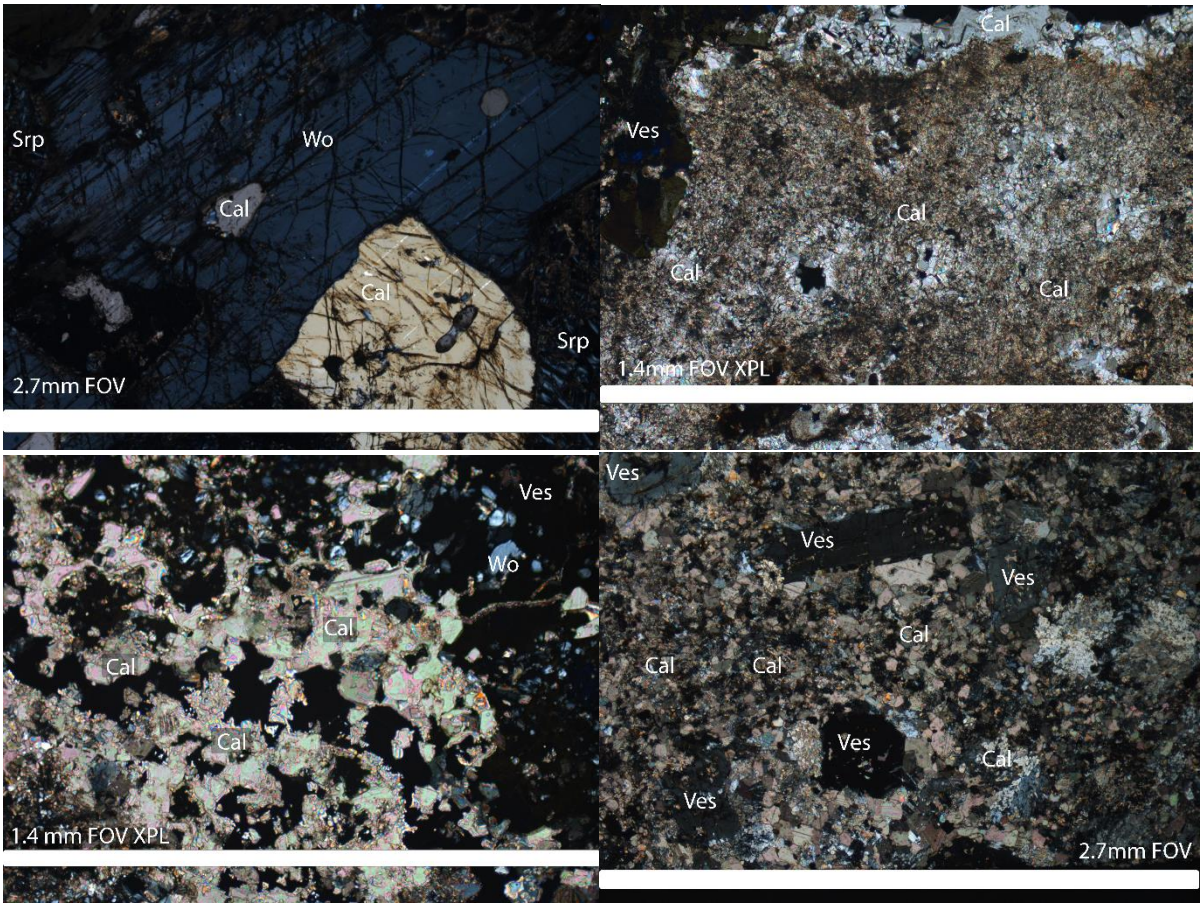

Figure 5. Photomicrographs of calcite from: sample 4 (top left, 15 meters from the pluton), sample 10 (top right, 21.7 meters from the pluton). sample 9 (bottom left, 28.3 meters from the pluton), and sample 8 (bottom right, 38.3 meters from the pluton). All photos are taken in XPL.

Wollastonite

The wollastonite changes from large and euhedral grains to subhedral grains that get smaller as the distance increases from the pluton (Figure 6). Wollastonite is only present in samples 4, 10, and 9. The wollastonite exhibits simple twinning in some crystals. This is a pure wollastonite. Its formula is $CaSiO_3$. The grain sizes vary from anywhere from 3 mm in length to as small as 0.1 mm in length. (See appendix VII).

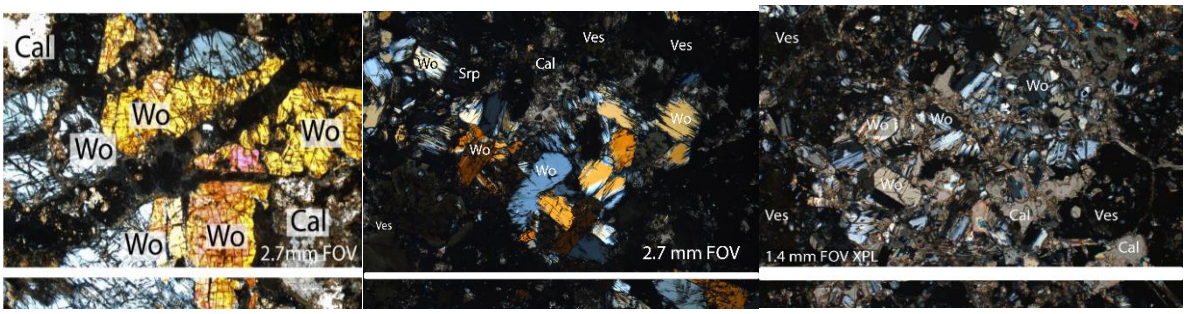

Figure 6. Photomicrographs of wollastonite from sample 4 (left microphotograph, 15 meters from the pluton), sample 10 (center microphotograph, 21.7 meters from the pluton). And sample 9 (right photomicrograph, 28.3 meters from the pluton). All photos are taken in XPL.

Phlogopite

Phlogopite has only been identified in sample 9, and features grains that are mostly <1mm in length with occasionally larger grain and are subhedral (Figure 7). The mica does not have pleochroism due to the lack of appreciable iron making it colorless.

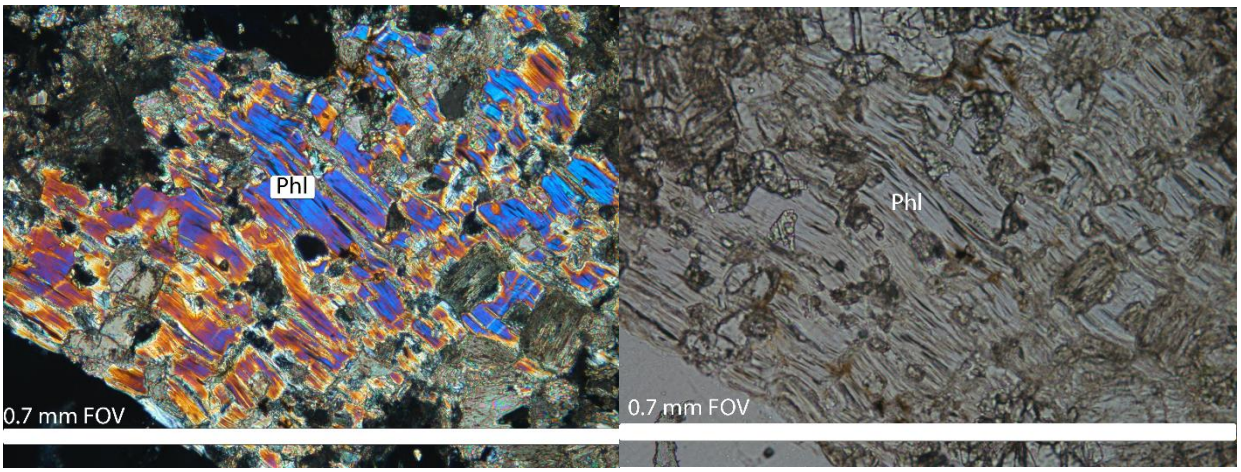

Figure 7. Photomicrographs (XPL and PPL) of the phlogopite in sample 9. There is a lack of pleochroism due to the lack of iron in the mica.

Mineral formulae for the phlogopite from WDS Analyses:

Phlogopite	$K\ Fe_{0.1}Mg_{2.7}Al_{1.4}Si_{2.8}O_{10}(OH)_2$
	$K\ Fe_{0.1}Mg_{2.8}Al_{1.4}Si_{2.8}O_{10}(OH)_2$
	$K_{0.9}Fe_{0.1}Mg_{2.7}Al_{1.4}Si_{2.8}O_{10}(OH)_2$

Pyrite

Pyrite is present in samples 10, 9, 8, 14 and 15. The pyrite grains are small, and 0.05mm in length at the largest. The pyrite is anhedral, opaque, and are bright yellow in reflected light (Figure 8). Overall, the pyrite is more abundant in the limestone samples than in the skarn.

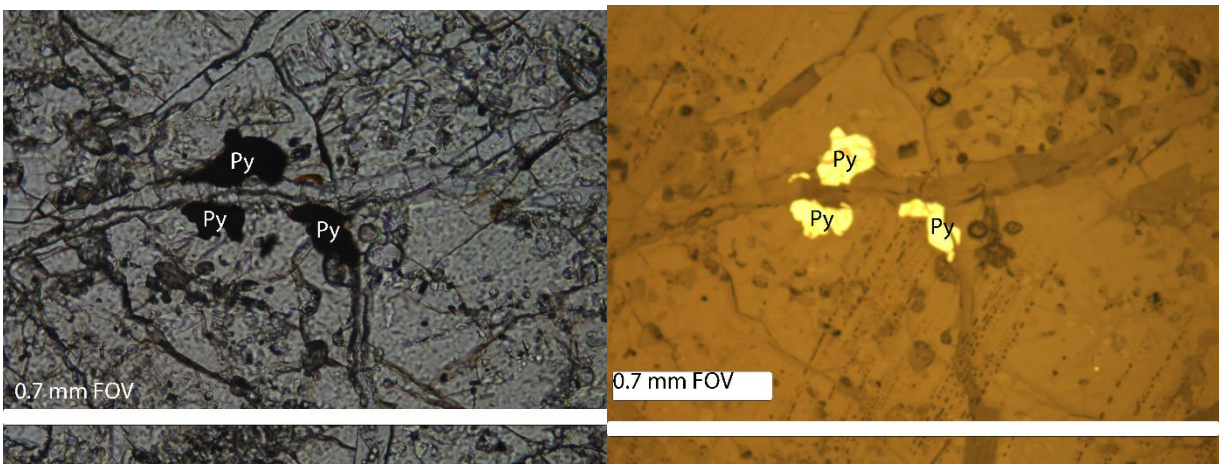

Figure 8. Pyrite photomicrographs (PPL and reflected light) from sample 9.

Grossular-andradite garnet

In sample 9 there is also grossular-andradite garnet (Figure 9). The garnets are colorless, euhedral and are <0.5 mm in length (Figure 14). The garnets are isotropic and high relief and are relatively inclusion-free.

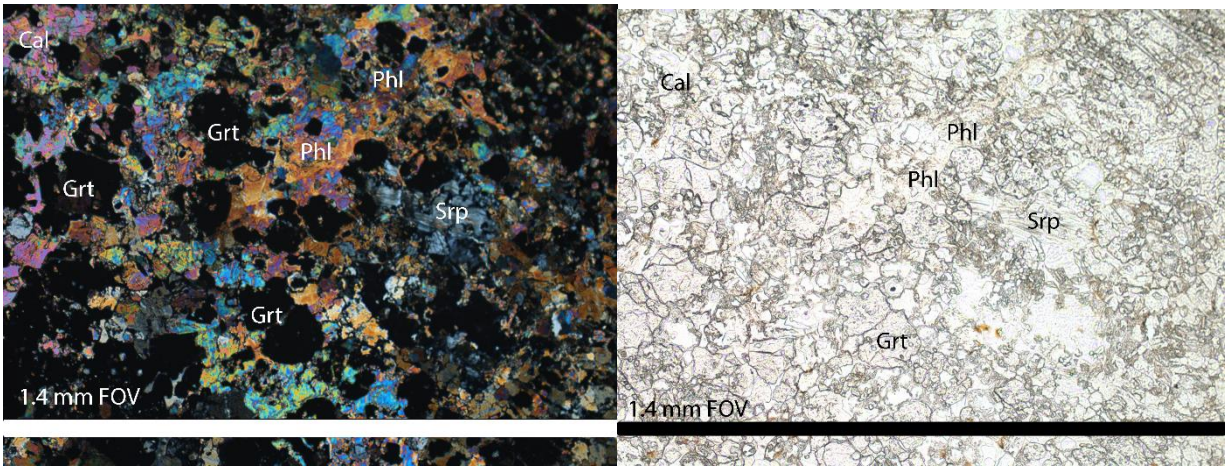

Figure 9. Photomicrographs (XPL and PPL) of Grossular-Andradite from sample 9.

Mineral formulae for grossular-andradite from WDS Analyses:

Grossular-andradite $Ca_3Fe_{0.7}Al_{1.3}Si_3O_{12}$

$Ca_3Fe_{0.5}Al_{1.5}Si_3O_{12}$

$Ca_3Fe_{0.7}Al_{1.3}Si_3O_{12}$

Scawtite

Scawtite is an unusual hydrous calc-silicate mineral present as subhedral diamond-shaped crystals. This retrograde metamorphic mineral has been documented to form in H_2O-CO_2 fluids that are water rich. This mineral has also been noted to form during the decarbonation of limestones (Kaprálik et al., 1984; Harker, 1965). The mineral formula for scawtite is $Ca_7Si_6O_{18}CO_3 \cdot 2H_2O$. It has a slightly higher Ca:Si ratio than wollastonite (Wollastonite has a 1:1 Ca:Si ratio while scawtite has a 7:6 Ca:Si ratio) (Figure 10 and appendices VII and VIII). Scawtite exhibits 1st order reds to upper 2nd order blue-green interference colors in XPL, is colorless in PPL, has low relief, and inclined extinction (Figure 11). This mineral was identified using Raman spectroscopy (Figure 12).

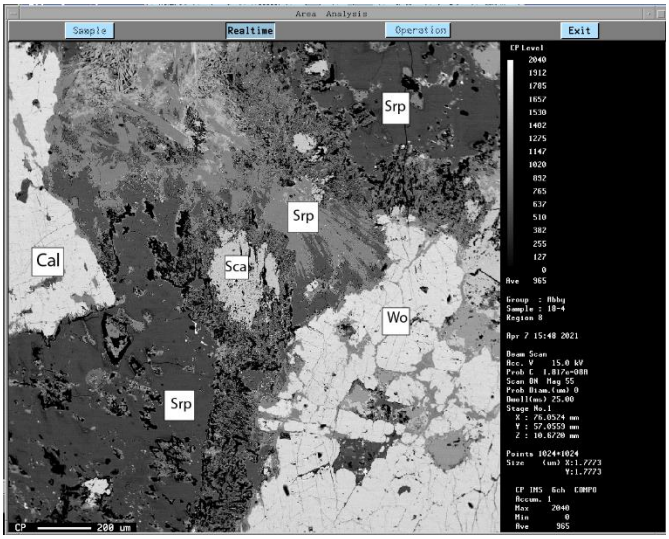

Figure 10. A BSE image noting how scawtite looks in relation to the other minerals present.

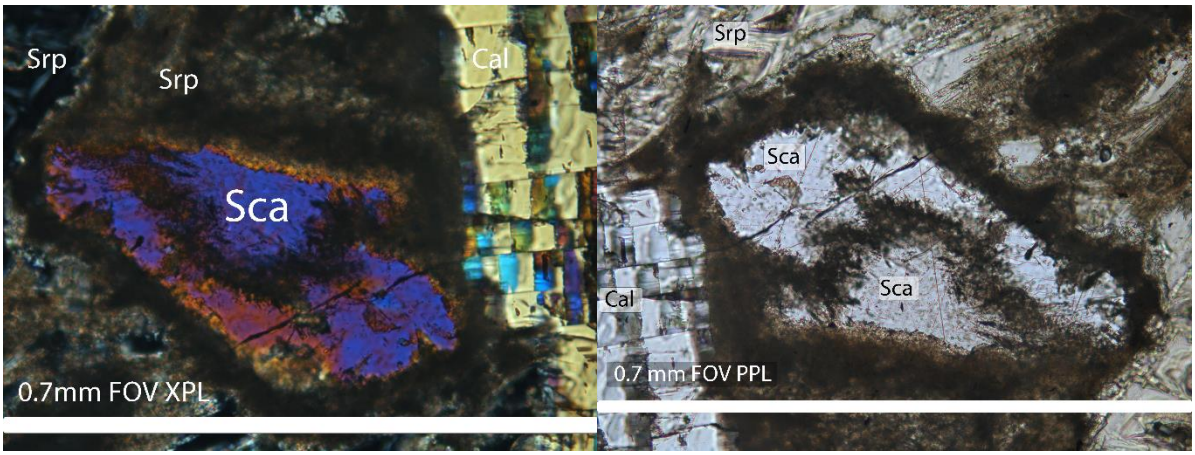

Figure 11. Photomicrographs (PPL and XPL) of scawtite from sample 4.

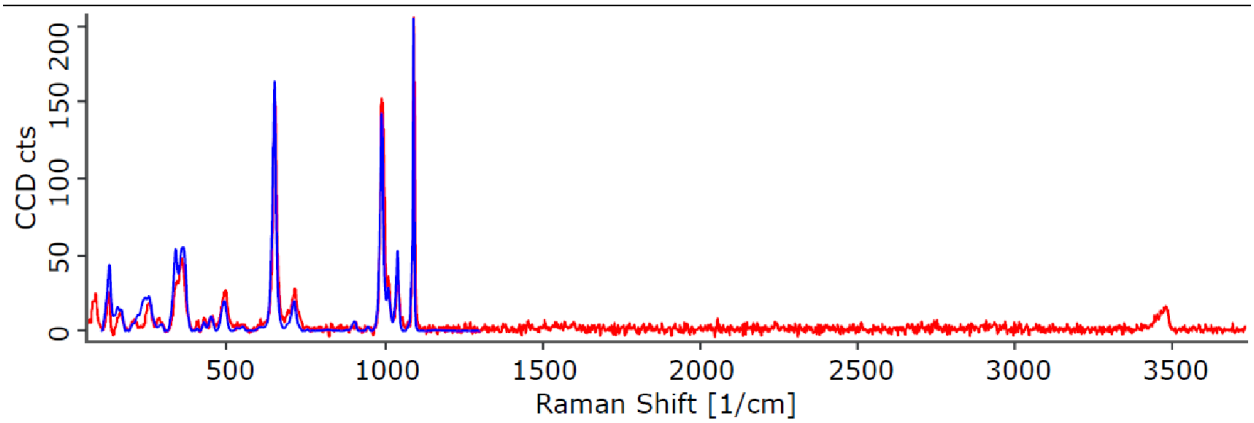

Figure 12. Raman spectrum of the scawtite, Red is the reference mineral, and the blue is the mineral analyzed in sample 4

Serpentine

Serpentine- group minerals chrysotile and lizardite are present in samples 9, 10, and 4 (Table 1). These minerals make up the majority of the matrix in samples, 4 and 10. The serpentine present is fibrous with elongate grains, and with no higher than 1st order white interference colors (Figure 13). No extinction angle or interference figure could be determined. These serpentines were confirmed with Raman spectroscopy (Figures 14 and 15).

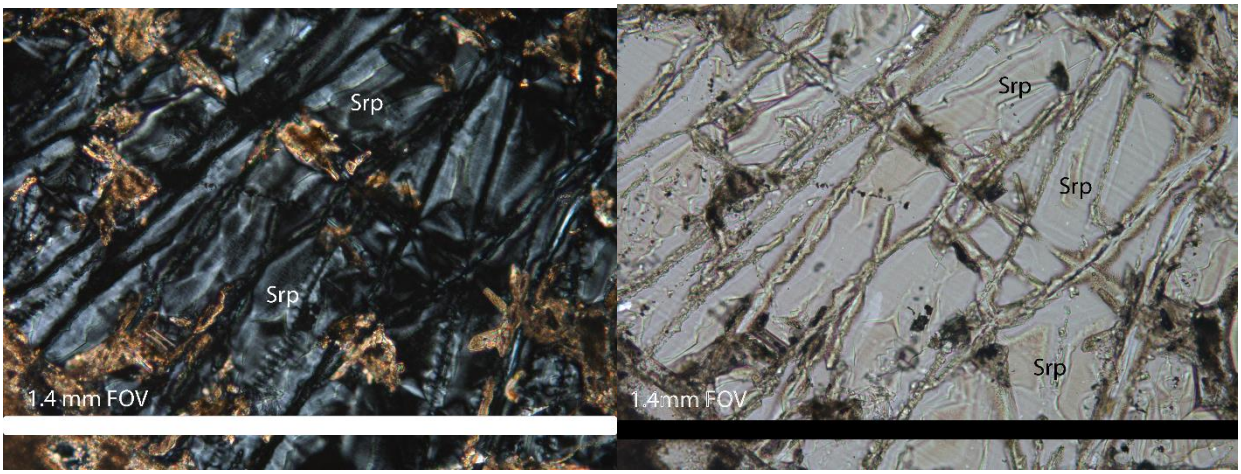

Figure 13. Photomicrographs (XPL and PPL) of the serpentine-group minerals from sample 4.

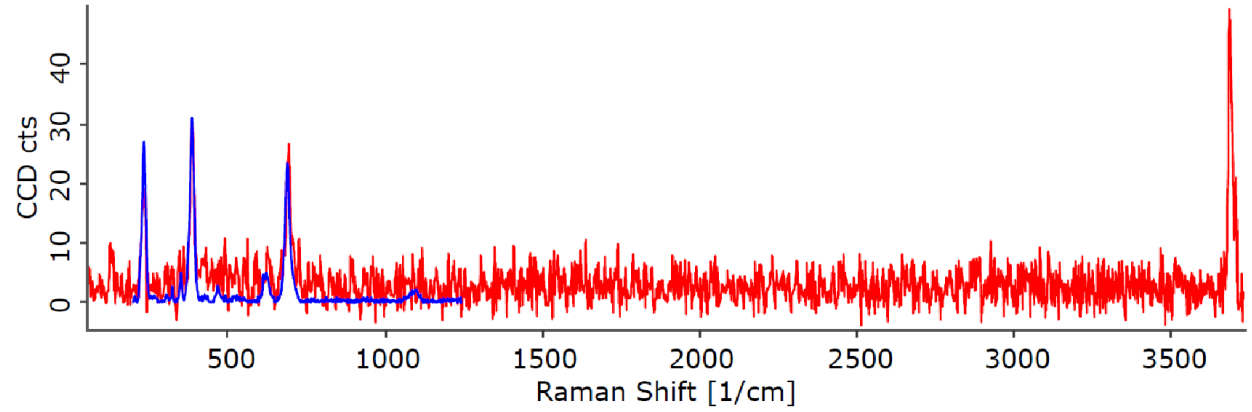

Figure 14. Raman spectrum of chrysotile, Red is the reference mineral, and the blue is the mineral analyzed in sample 4.

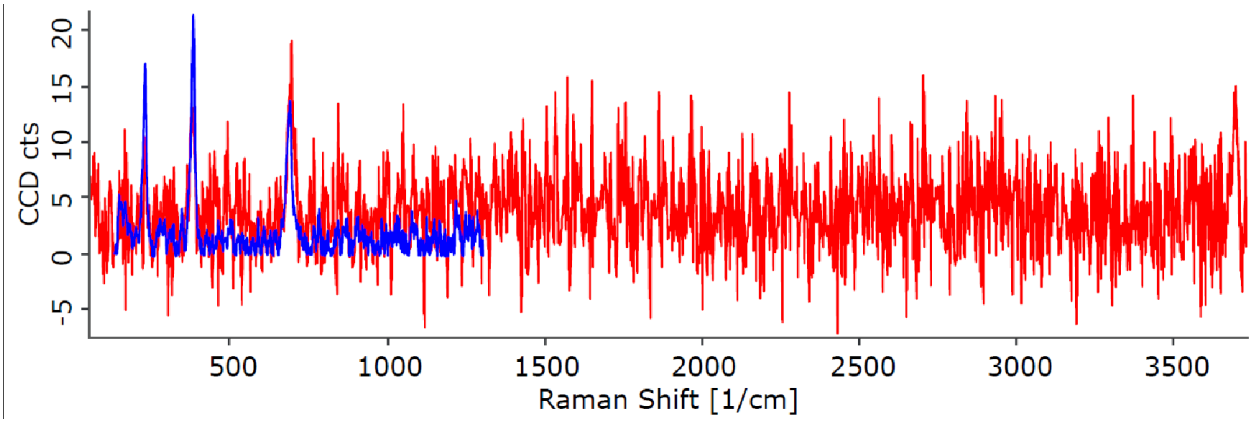

Figure 15. Raman spectrum of lizardite, Red is the reference mineral, and the blue is the mineral analyzed in sample 4.

Andradite-schorlomite-grossular garnet

Andradite-schorlomite-grossular garnets are present as euhedral equant grains. This unusual garnet is yellow in PPL and is isotropic (Figure 16). This mineral is found only in sample 9. This mineral contains Ti, Fe, Si, Mg and Ca in its composition. Identification of this mineral was difficult due to the complex chemistry (Figure 17 also see appendices VII). Raman spectroscopy was used to identify this unusual type of garnet.

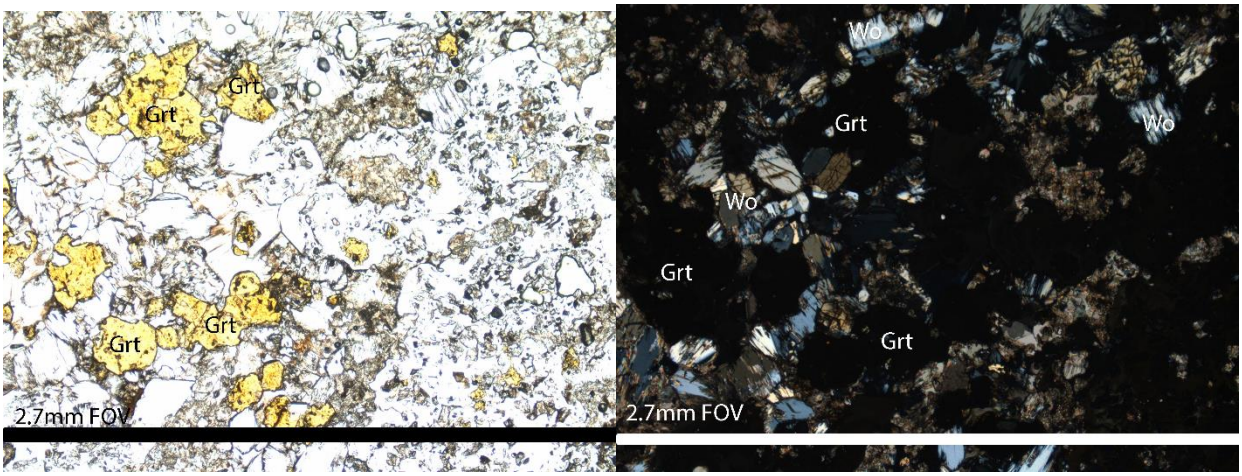

Figure 16. Photomicrographs (PPL and XPL) of andradite-schorlomite-grossular garnets in sample 10.

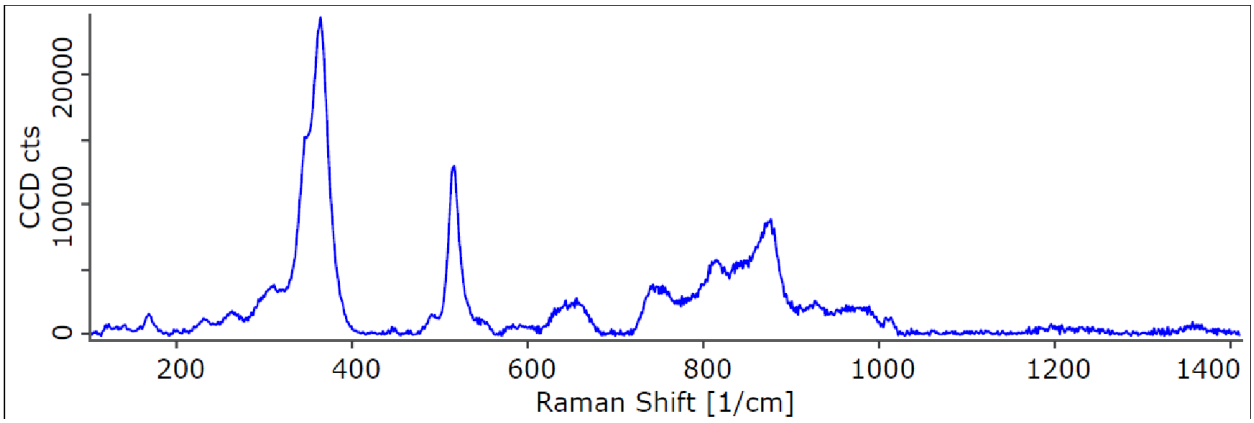

Figure 17. Raman spectrum of the andradite-schorlomite-grossular garnet.

Mineral formula for Andradite-schorlomite-grossular from WDS

$Ca_3Fe_{1.3}Al_{0.6}Si_{2.5}Ti_{0.6}O_{12}$

Monticellite

Monticellite was only found in sample 5, This skarn was not found along the primary traverse taken but at a smaller rooftop pendant skarn also at the pluton. This mineral is colorless in PPL, has interference colors no higher than 1st order reds in XPL, and has inclined extinction (Figure 18).

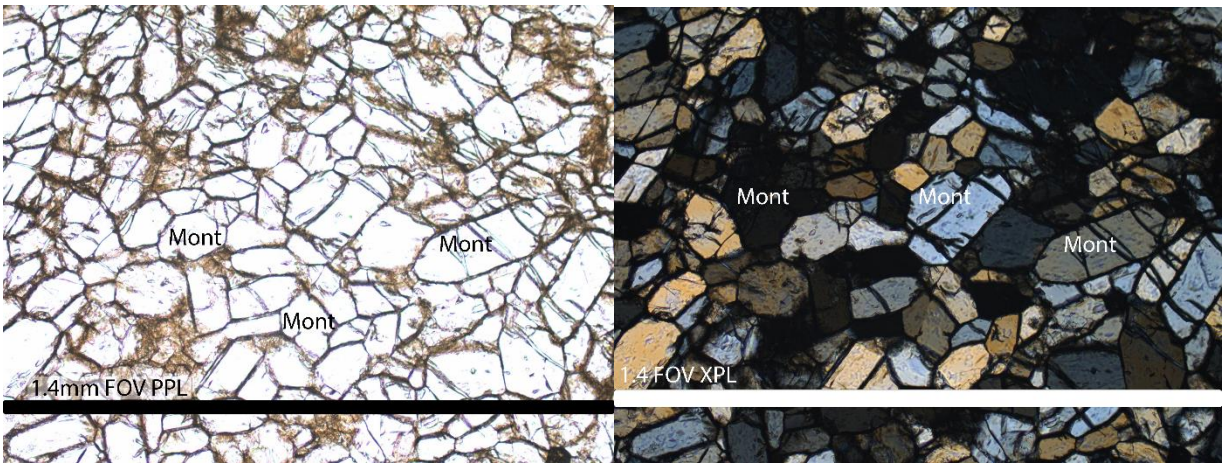

Figure 18. Photomicrographs (PPL and XPL) of monticellite from sample 5.

Retrogressed mineral evidence

Textures observed using the microscope suggest that some of the minerals found in the skarns were formed during retrogression during cooling of the pluton. Pseudomorphs consisting of serpentine and calcite suggest that either diopside or forsterite may have been present at peak P-T conditions (see figure 19).

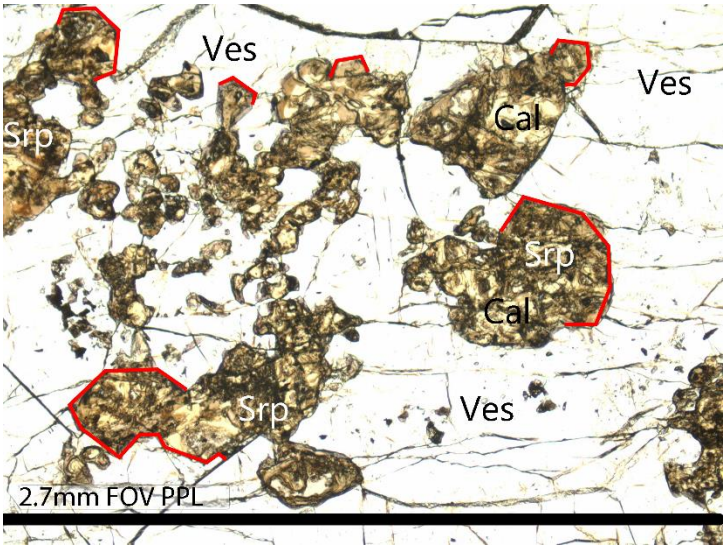

Figure 19. A Photomicrograph (PPL) from sample 4 showing retrogressed mineral relationships of the serpentine and calcite. Red is highlighting the shapes that mimic original prograde minerals.

5.2 Geochemistry

The most abundant chemical components of the skarns are CaO, SiO_2, Al_2O_3, Fe_2O_3, and MgO. These elements typically vary in concentration as the distance changes from the pluton. However, for most elements there is no systematic increase or decrease as a function of distance from the pluton (Figure 20). Samples 10, 9, and 8 are the highest in CaO from all samples. There is no significant variation in the Al_2O_3, or Fe_2O_3 as the distance increases from the pluton.

This indicates that the changes in mineralogy are due to fluid movement rather than large bulk chemistry changes of the rocks. The MgO increases in the two samples closest to the pluton. The LOI decrease from the pluton suggests that there is an overall decrease in volatiles due to skarn formation. The loss of ignition (LOI) from the XRF data shows the volatile content released from the rock powder when it is heated in the oven prior to XRF analysis. These are minerals with H_2O and CO_2 bound in their crystal structure.

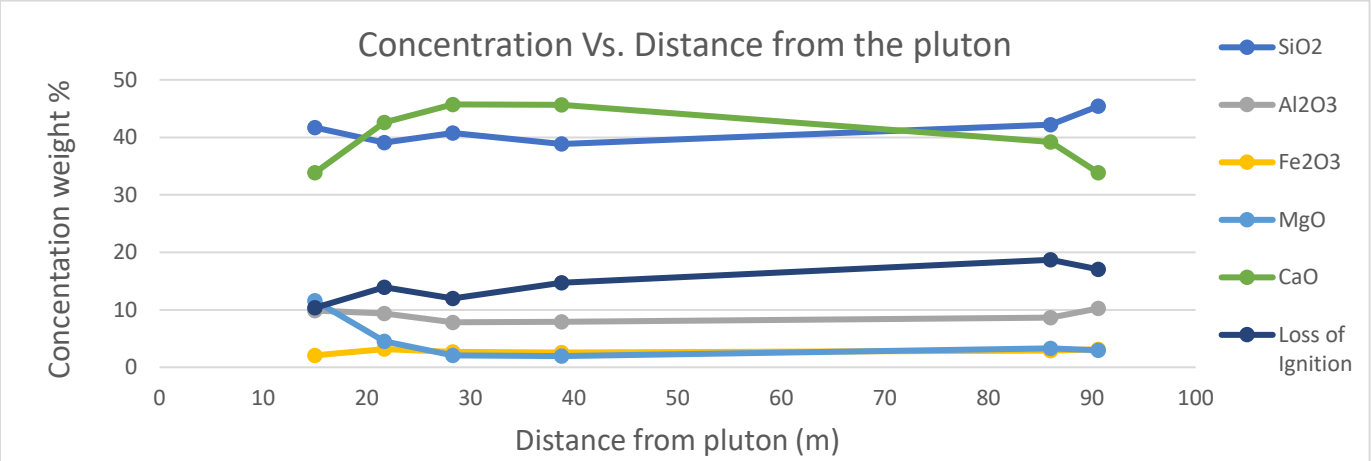

Figure 20. A plot of Bulk-rock XRF data vs. distance from the pluton. Sample 4 is 15 meters from pluton, sample 10 is 21.7 meters from pluton, sample 9 is 28.3 meters from pluton, and sample 8 is 38.3 meters from the pluton.

5.3 Stable isotope analysis

The $\delta^{18}O$ values in the samples indicate whether the fluid came from the country rock, or pluton as they have different isotopic signatures. Fluid derived from igneous plutons will have 6 to 11 ‰VSMOW for the $\delta^{18}O$, and for $\delta^{13}C$ 6 to 10 ‰ PDB (Figure 22; Baumgartner and Valley, 2001). If the fluid originates from the country rock the $\delta^{13}C$ will be close to 0 ‰ for a marine limestone, and for $\delta^{18}O$, the range will be anywhere from 22 to 28 ‰ (Shieh, and Taylor, 1969). and will not change since the country rock is the protolith. These measurements would then demonstrate whether the metasomatism occurred due to the fluid coming from the pluton or country rock, or if both are playing a factor to some extent.

The stable isotope analysis shows that there is different isotopic composition when comparing the skarns to the protolith. This indicates that there is an isotopic alteration due to fluids (Figure 21). When the $\delta^{18}O$ and $\delta^{13}C$ are plotted against each other, four of the samples fall within the range of compositions expected from Rayleigh volatilization (Figure 22). The amount of volatilization (indicated by the degree of change in $\delta^{18}O$ and $\delta^{13}C$) is not related to distance from the pluton (Table 2 and figure 22). One of the samples falls outside the range predicted for Rayleigh volatilization however this does suggest that fluids derived from the pluton shifted the isotopic composition of this sample (sample 4). Overall, this data indicates that both devolatilization and interaction with fluids derived from the nearby pluton altered the isotopic composition of the skarn rocks.

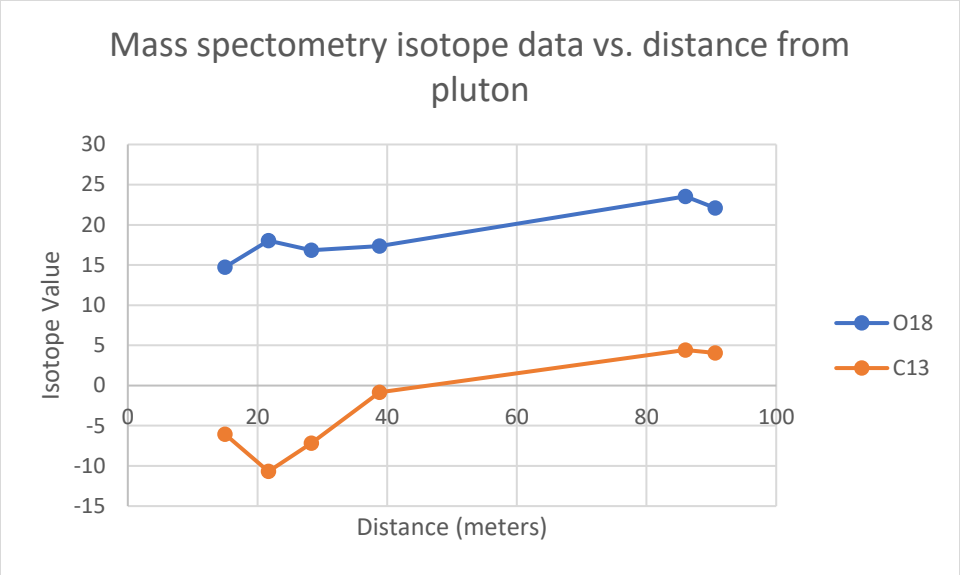

Figure 21. A plot of isotope value vs. distance from pluton comparing the δ ^{18}O and δ ^{13}C to the distance from the pluton.

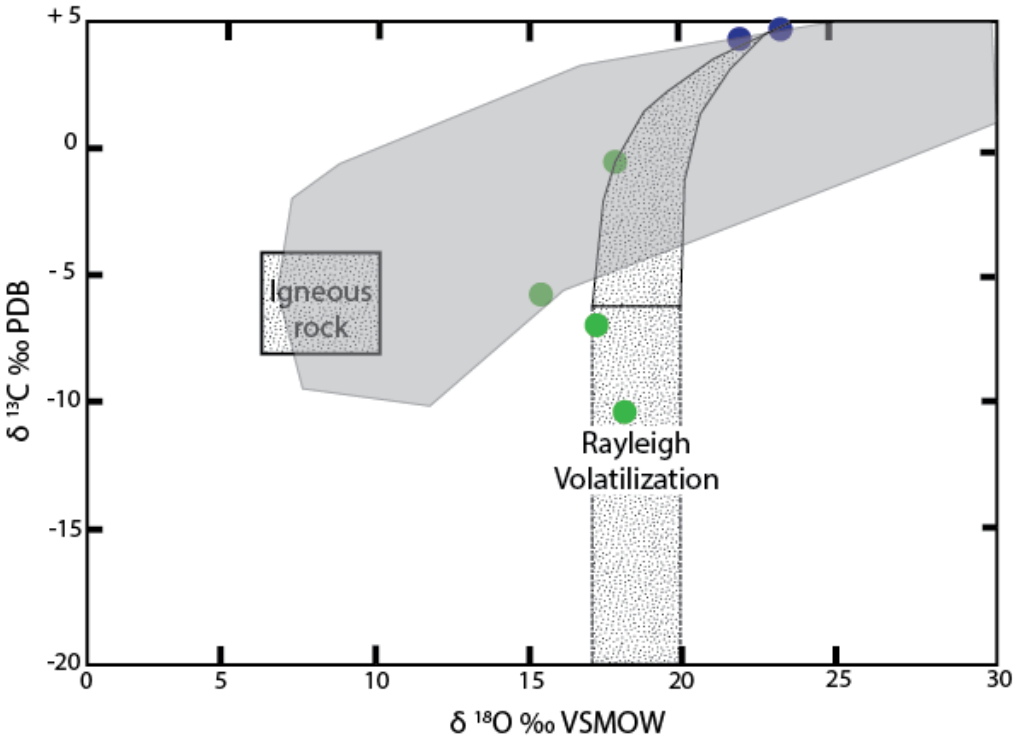

Figure 22. A δ ^{18}O vs. δ ^{13}C plot comparing the measured isotopic compositions of the protolith limestone in blue and the skarn samples in green to the isotopic compositions expected during Rayleigh devolatilization and the isotopic compositions of igneous rocks (adapted from Baumgartner and Valley, 2001). The grey field represents other studies documented that interpreted the pluton-derived fluids interacting with carbonate rock.

Measured stable isotope conditions

Sample	$\delta^{18}O$ (‰)	STD for $\delta^{18}O$	$\delta^{13}C$ (‰)	STD for $\delta^{13}C$
Sample 4	14.74	0.20	-6.06	0.33
Sample 10	18.02	0.14	-10.69	0.11
Sample 9	16.83	0.07	-7.18	0.09
Sample 8	17.36	0.19	-0.85	0.02
Sample 14	23.54	0.06	4.43	0.08
Sample 15	22.09	0.02	4.04	0.07

Table 2. The isotopic values and standard deviation from each of the limestones and skarns. Green indicates skarn samples; blue indicates limestone samples.

6. Discussion

6.1 Immobile reference frame

To determine whether trace elements have increased or decreased due to metamorphism, one must start with determining an immobile reference frame due to the closure problem (Ague & van Haren, 1996). The closure problem describes the issue with open systems which is with significant mass addition or loss of one element, the concentration of the other elements will decrease (or increase) without any loss, due to concentrations being reported as percentages. To determine an immobile reference frame the average of the two unmetamorphosed limestone samples were used to represent the protolith composition (Appendix IX). Using the concentration ratio. C'/C_0, where C' is the concentration of the given element in the skarn and. C_0 is the concentration of the same element in the average protolith (Figure 23). A completely immobile element would have a concentration ratio of 1. Immobile reference elements are elements that are commonly considered immobile meaning that they are not elements typically commonly known to travel with fluid in metamorphic settings (Ague, 1994). Examples of immobile elements include Al, Zr, Ti, REEs, Ni, and Cr (Penniston-Dorland and Ferry, 2008; Ague 1994; Penniston-Dorland et al., 2014). There is significant variability in Ti, Ni, and Zr in the skarn samples, therefore they were not considered further for the immobile reference frame. Considering other elements, Al, Sc, Ga, and Fe these elements were further analyzed and were determined to be immobile because their concentration ratios were within uncertainty of each other (see Appendix X for results). The concentration of those immobile elements shows that there is no overall mass loss or gain since the concentration ratios of these immobile elements are within the uncertainty of $\log(C'/C_o) = 0$.

6.2 Element mobility and mass change

The two limestone protoliths were compared to determine the variability of the protolith (see the results of this analysis in Appendix XI). The $\log(C'/C_o)$ values range resulting from this comparison -0.38 to +0.34. This range was used in the analysis of figure 23 as the upper and lower bounds of the natural rock variability. Any of the elements from the four skarn samples

that fall between the natural rock variability are considered immobile for that sample. Elements for which most of the skarn ratios fall outside of this reference frame are considered to be mobile. If they fall above the reference frame they are added to the rock during metamorphism. If they fall below, they are removed during metamorphism. Based on this analysis Sr, Ba, Pb, and K are considered mobile elements and they are removed during metamorphism since they fall below the reference frame (Figure 23). See figure 24 to see the % mass change of these elements. For the three skarn samples closest to the pluton (4, 10 and 9) exhibit consistent mass changes. These samples show consistent loss in K, Rb, Ba, and Sr. Pb is lost in two of these samples (samples 9 and 10) but gained in one (sample 4). Sample 8 shows different behavior, with loss in Pb, and relatively small losses in K, and Rb (within limestone protolith variability), and gains in Sr and Ba. Mass losses range up to 100% (Figure 24). The increase in MgO in the samples adjacent to the pluton is also observed in this analysis with the MgO in sample 4 falling outside the range of protolith variability. This increase may be due to the addition of Mg of fluids derived from the pluton (Figure 23).

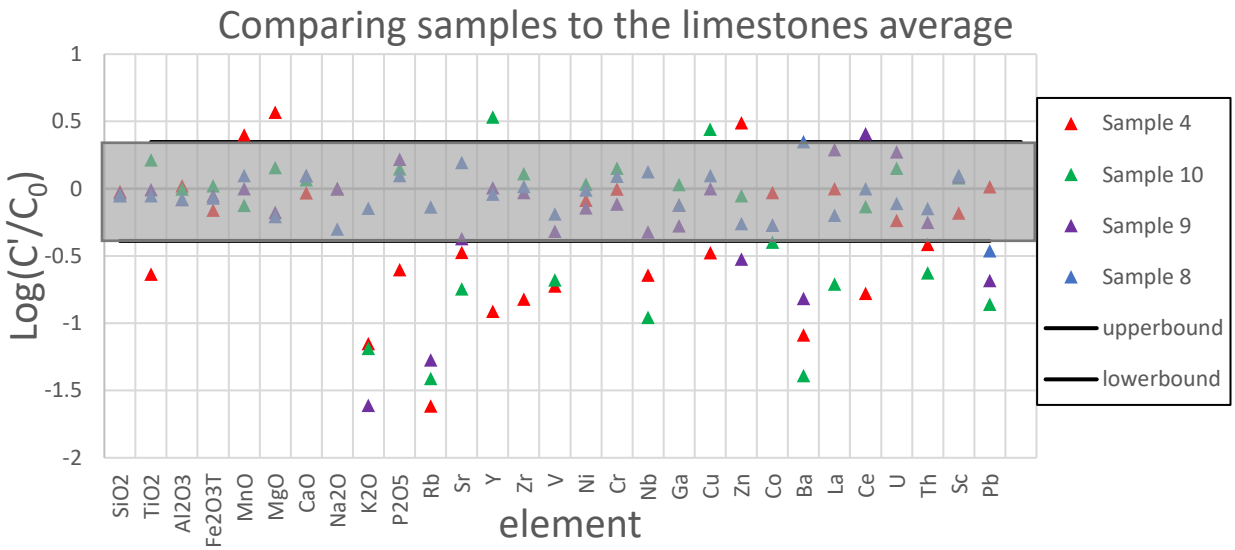

Figure 23. Concentration ratios (log scale) for major and minor trace elements for the skarns. The black lines and grey box are the natural variability of the limestones collected.

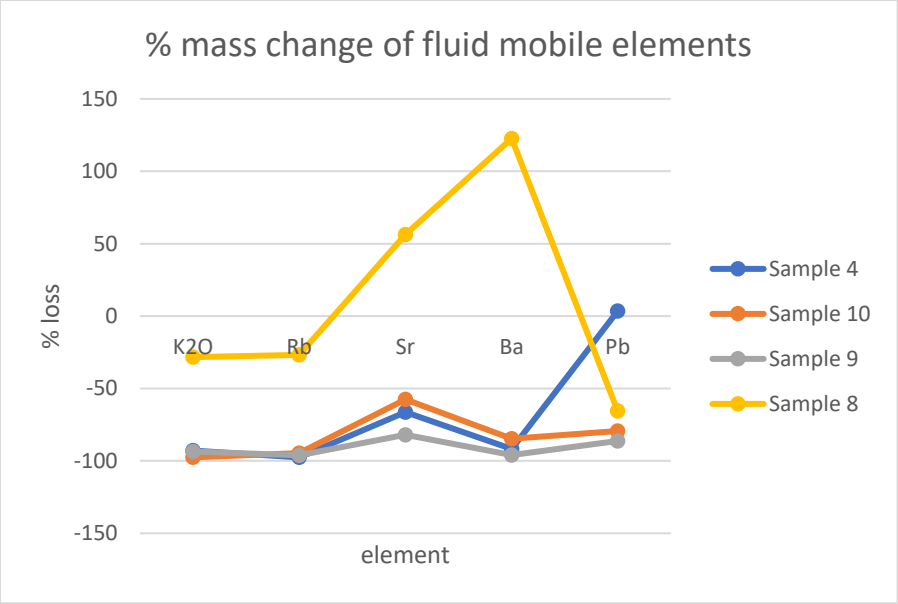

Figure 24. A plot of percent mass change of the fluid mobile elements.

6.3 Fluid composition

Thermodynamic analysis using minerals present in the rocks can indicate the composition of the fluid in equilibrium with the rocks. Assumptions for this analysis have been made about the pressure of the metamorphism. The pressure is estimated to be no more than 0.05 GPa based on observations of the shallow emplacement of the pluton (Fenn, 1968). Fenn (1968) calculated the pressure by assuming equilibrium between K-feldspar and olivine in a lamprophyre associated with the pluton to obtain the pressure. The product minerals wollastonite, and vesuvianite coexist with grossular and calcite in sample 9. These minerals were used to infer the reaction of grossular, diopside and calcite to form vesuvianite and wollastonite. Perple_X (Connolly, 2009) was used to calculate the T- X_{CO2} conditions for this reaction shown in figure 26. The presence of monticellite in sample 5 was used to infer a possible reaction of diopside, forsterite and calcite to produce monticellite, and the T- X_{CO2} conditions for this reaction are also shown in figure 26. These reactions indicate fluid equilibrium is X_{CO2} <0.27 (the shaded green field in figure 26). The presence of monticellite suggests an even lower X_{CO2} however, this is from a different outcrop and was not collected with the traverse (Figure 2). This analysis suggests there is a water component of at least 73%.

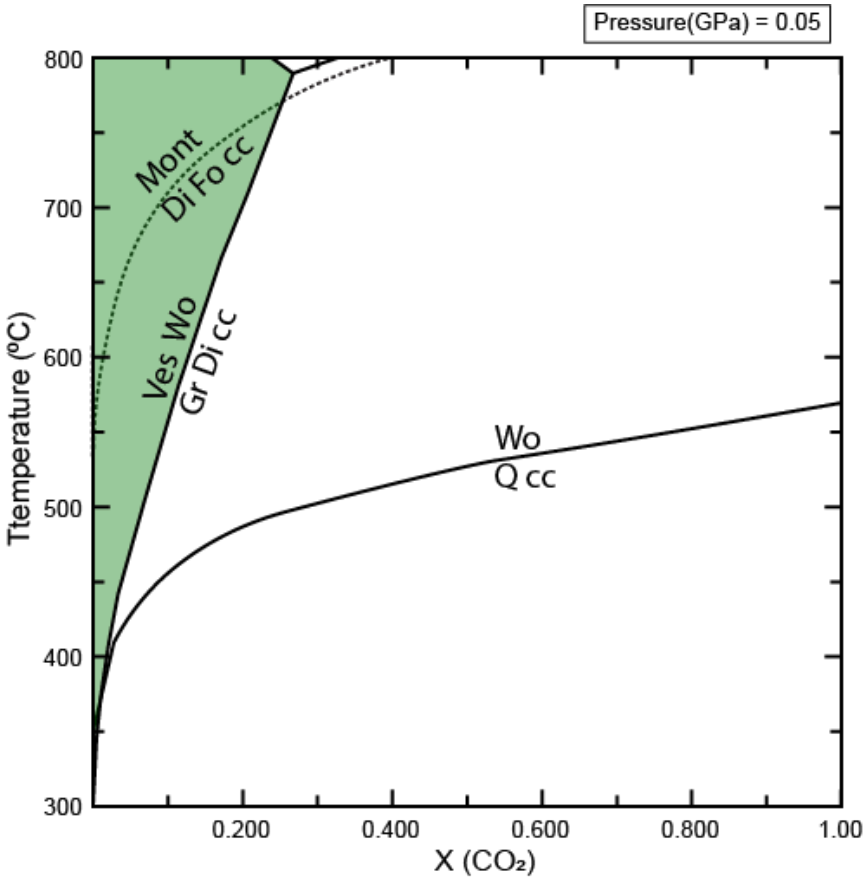

Figure 26. A Temperature vs. X-CO_2 diagram made using Perple_X with the Holland and Powell 1998 database. The green indicates the field where the proposed phase assemblage.

6.4 Perple_X Interpretations

Perple_X (Connolly, 2009) calculations using Bulk XRF data were unsuccessful, most pseudosections made only displayed 1 to 3 minerals present in each sample and included minerals that were not observed in any of the samples. This may have been due to some disequilibrium occurring in the rock, and due to many minerals desired for in the Holland and Powell (1998) database do not contain enough thermodynamic information for the range of mineral compositions found in the rocks. This may also reflect that many of the unusual minerals in these rocks are solid solutions which the Holland and Powell (1998) database only has endmember composition data for. To see the unsuccessful results of Perple_X calculations see appendix XI.

7. Conclusion

The work to date reveals complex mineralogy of the samples. All the skarn samples contain calcite and vesuvianite. Other skarn minerals found include grossular-andradite, wollastonite, serpentines, pyrite, and phlogopite. There are some more exotic minerals appearing as well such as monticellite, andradite-schorlomite-grossular and scawtite, some of which have not been well studied or previously documented at this locality. The presence of vesuvianite and

wollastonite in multiple samples suggests a H_2O-rich fluid of at largest X_{CO2} <0.27. The presence of scawtite suggests that a water rich fluid was present during retrogression metamorphism as well. The loss of the elements of K, Sr, Pb, and Ba by at least 72% indicate for most skarn samples indicate that H_2O-rich fluid changed the chemistry of the rocks during the metamorphism of the skarn.

There is a significant increase of MgO content of the two skarn samples closes to the pluton compared to the limestones (Figure 20) The amount of MgO in sample 4 is above the natural variability of the limestones suggesting that MgO was added to this skarn sample, potentially by fluids derived from the pluton. The $\delta\ ^{18}O$ and $\delta\ ^{13}C$ of the skarns are consistent with fluids derived from the pluton along with devolatilization during skarn formation.

8. Acknowledgments

I would like to thank my advisor, Dr. Sarah Penniston-Dorland, the head detective of the Super Petrology Detectives, for helping with the investigative detective work for so many papers, revisions, and supporting this kitchen sink research project. I thank Dr. Piccoli, for providing EPMA data on the thin sections, helping me keep track and not get overwhelmed when things got down to the wire. I thank Dr. Evans for running my samples and providing data on his mass spectrometer. I thank Dr. Igor Puchtel for assisting with solving shatterbox catastrophes. I'd also like to thank Dr. Andrew Steele for allowing me to visit and supervise the use of the Raman at Carnegie Institute. I'd like to thank Dr. Stan Mertzman at Franklin and Marshall college for providing the XRF analysis. And finally, I'd like to thank Dr. Hugo van Schrojenstein Lantman for giving me the idea to use Raman, and for teaching and helping me troubleshoot Perple_X, the T-X diagrams would not have been able to be made without his patience and expertise.

9. Bibliography

Bibliography

Ague, J. J. (1994). Mass transfer during Barrovian metamorphism of pelites, south-central Connecticut; I, evidence for changes in composition and volume. *American Journal of Science, 294*(8), 989-1057. doi:10.2475/ajs.294.8.989

Ague, J. J., & van Haren, J. L. (1996). Assessing metasomatic mass and volume changes using the bootstrap, with application to deep crustal hydrothermal alteration of marble. *Economic Geology*, *91*(7), 1169–1182. https://doi.org/10.2113/gsecongeo.91.7.1169

Ahmed-Said, Y., & Leake, B. E. (1996). The conditions of metamorphism of a grossular—wollastonite vesuvianite skarn from the Omey granite, Connemara, western Ireland, with special reference to the chemistry of vesuvianite. *Mineralogical Magazine*, *60*(401), 541–550. https://doi.org/10.1180/minmag.1996.060.401.01

Baumgartner, L. P., & Valley, J. W. (2001). Stable isotope transport and contact metamorphic fluid flow. *Reviews in Mineralogy and Geochemistry*, *43*(1), 415–467. https://doi.org/10.2138/gsrmg.43.1.415

Bean, C. L., 1981. A geochemical study of the North Doherty Intrusive Complex, Jefferson County, Montana. MA thesis, Indiana University.

Berger, B. R., Hildenbrand, T. G., & O'Neill, M. J. (2011). Control of Precambrian basement deformation zones on emplacement of the Laramide Boulder batholith and Butte mining district, Montana, United States. *US. Geological Survey*, 1–39. https://doi.org/10.3133/sir20115016

Brady, J. B., Burger, R. H., Cheney, J. T., & Harms, T. A. (Eds.). (2004). *Precambrian geology of the Tobacco Root Mountains, Montana*. Geological Society of America.

Connolly, J.A.D., 2009. The geodynamic equation of state: what and how. *Geochemistry, Geophysics, Geosystems* vol. 10 Q1014 doi:10.1029/2009GC002540

Deer, W. A., Howie, R. A., & Zussman, J. (1997). Vesuvianite (Idocrase). In *Rock-forming minerals* (pp. 113–120). chapter, The Geological Society.

Einaudi, M. T., & Burt, D. M. (1982). Introduction; terminology, classification, and composition of skarn deposits. *Economic Geology, 77*(4), 745-754. doi:10.2113/gsecongeo.77.4.745

Evans, M. N., Selmer, K. J., Breeden, B. T., Lopatka, A. S., & Plummer, R. E. (2016). Correction algorithm for online continuous flow δ13C and δ18O carbonate and cellulose stable isotope analyses. *Geochemistry, Geophysics, Geosystems*, *17*(9), 3580–3588. https://doi.org/10.1002/2016gc006469

Fenn, P. M. (1968). *Feldspar thermal states as an indicator of relative ages in the Mt. Doherty igneous complex*. Unpublished manuscript, Massachusetts Institute of Technology, Boston.

Harker, R. I. (1965). Scawtite and its synthesis. *Mineralogical Magazine and Journal of the Mineralogical Society*, *34*(268), 232–236. https://doi.org/10.1180/minmag.1965.034.268.18

Holland, T. J., & Powell, R. (1998). An internally consistent thermodynamic data set for phases of Petrological Interest. *Journal of Metamorphic Geology*, *16*(3), 309–343. https://doi.org/10.1111/j.1525-1314.1998.00140.x

Kaprálik, I., Števula, L., Petrovič, J., & Hanic, F. (1984). Study of the system CaO-SiO_2-CO_2-H_2O in relation to scawtite under hydrothermal conditions. *Cement and Concrete Research*, *14*(6), 866–872. https://doi.org/10.1016/0008-8846(84)90013-9

Meinert, L. D. (1992). Skarn and Skarn Deposits. *Geoscience Canada*, *19*(4), 145-162.

Meinert, L. D., Dipple, G. M., & Nicolescu, S. (2005). World skarn deposits. *Economic Geology, 100*, 229-336. doi:10.5382/av100.11

Penniston-Dorland, S. C., & Ferry, J. M. (2008). Element mobility and scale of mass transport in the formation of quartz veins during regional metamorphism of the Waits River Formation, East-central Vermont. *American Mineralogist, 93*(1), 7-21. doi:10.2138/am.2008.2461

Penniston-Dorland, S. C., Gorman, J. K., Bebout, G. E., Piccoli, P. M., & Walker, R. J. (2014). Reaction rind formation in the Catalina Schist: Deciphering a history of mechanical mixing and metasomatic alteration. *Chemical Geology, 384*, 47-61. doi:10.1016/j.chemgeo.2014.06.024

Shieh, Y. N., & Taylor Jr, H. P. (1969). Oxygen and carbon isotope studies of contact metamorphism of carbonate rocks. *Journal of Petrology, 10*(2), 307-331.

White, R. W., Powell, R., & Johnson, T. E. (2014). The effect of Mn on mineral stability in metapelites revisited: New A-X relations for manganese-bearing minerals. *Journal of Metamorphic Geology, 32*(8), 809–828. https://doi.org/10.1111/jmg.12095

Whitney, D. L., & Evans, B. W. (2010). Abbreviations for names of rock-forming minerals. *American Mineralogist, 95*(1), 185-187. doi:10.2138/am.2010.3371

10. Appendix

I. Hand sample descriptions and photos

Sample 4

Sample 4 is a skarn and is the closest to the pluton along the traverse. This sample features large subhedral vesuvianite porphyroblasts, that are about 1.5mm in length, they make up about 70% of the hand sample. The sample also features some euhedral calcite grains as well that are about 0.5mm in length. Calcite and other matrix minerals make up about 30% of the rest of the sample. Due to the high amount of vesuvianite, it also very brittle

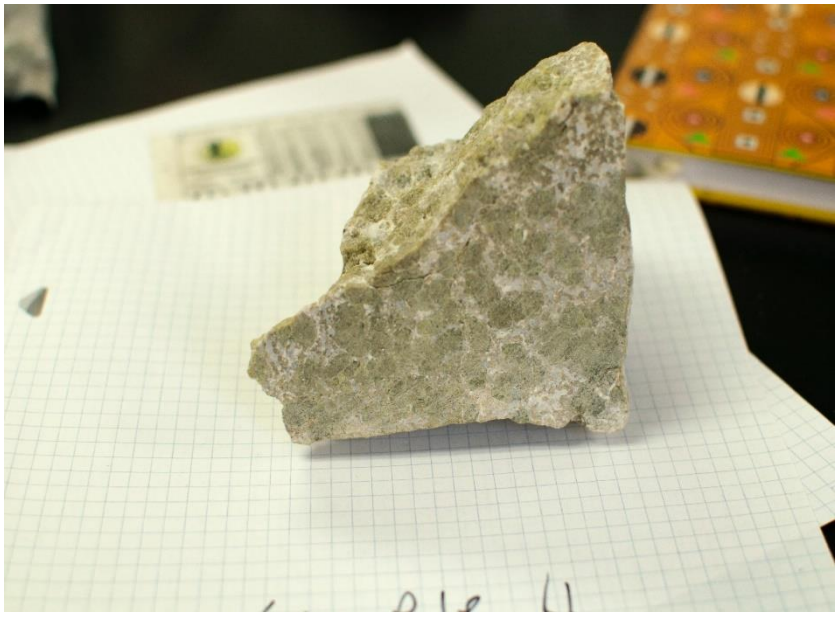

Figure 27. hand sample 4 photo.

Sample 10

Sample 10 is a skarn, that is much finer-grained than 18-4. This sample is light green, on the unweathered surfaces. There is a small black mineral appearing in hand sample that is about 0.01mm in length This mineral makes up about <1% of the hand sample. The subhedral calcite and other matrix minerals make up about 50% of the hand sample. Vesuvianite is present in the rock, and are much smaller than 18-4, as they are about 0.1mm in length. This sample is less brittle than sample 18-4 due to there being less vesuvianite. Vesuvianite makes up about 50% of the hand sample.

Figure 28. sample 10 hand sample photo.

Sample 9

Sample 9 a skarn, is a very fine-grained, and is slightly yellow in color. Vesuvianite makes about 35% of the hand sample and most grains are less than 0.1mm in length. Calcite and other matrix minerals make about 65% of the hand sample, and most grains are subhedral. There are calcite veins running through this hand sample.

Figure 29. hand sample 9 photo.

Sample 8

Sample 8 is a skarn and is the finest grained of the samples. This sample is the furthest from the pluton and likely represents the protolith of the metamorphosed rocks. This sample is the darkest in color of the samples and It is dark grey in color. No vesuvianite can be seen in this sample on the surface. This sample seems to be 100% calcite and the other matrix minerals. Calcite veins are also present in this hand sample.

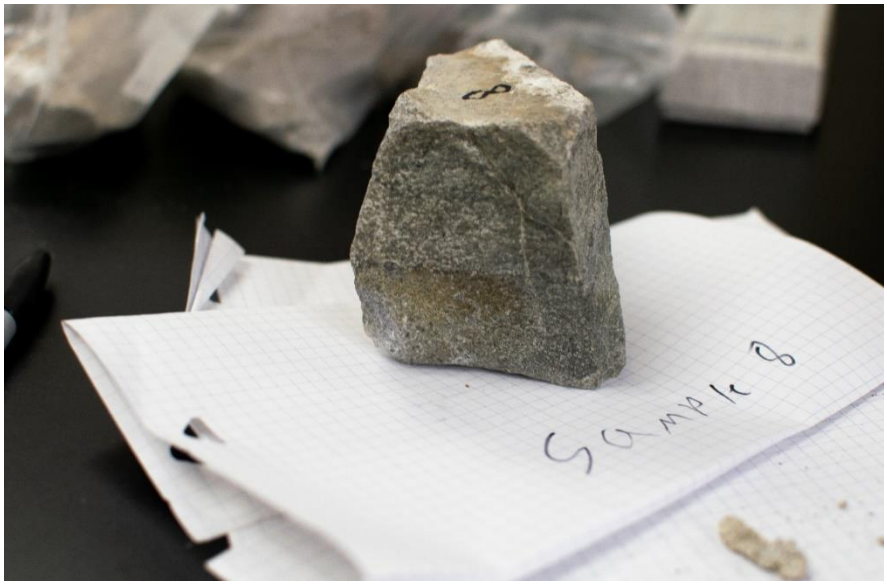

Figure 30. hand sample 8 photo.

Sample 14

Sample 14 is a dark grey muddy micritic limestone. This sample is from the lower part of the Lodgepole's formation based on its color.

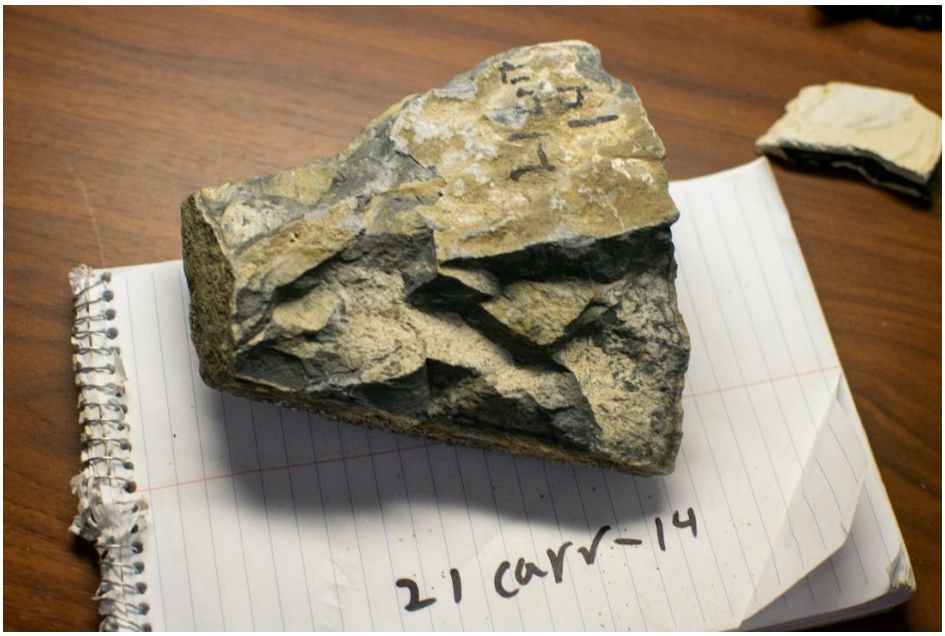

Figure 31. Sample 14 hand sample photo

Sample 15

Sample 15 is a dark grey muddy micritic limestone. This sample is from the lower part of the Lodgepole's formation based on its color.

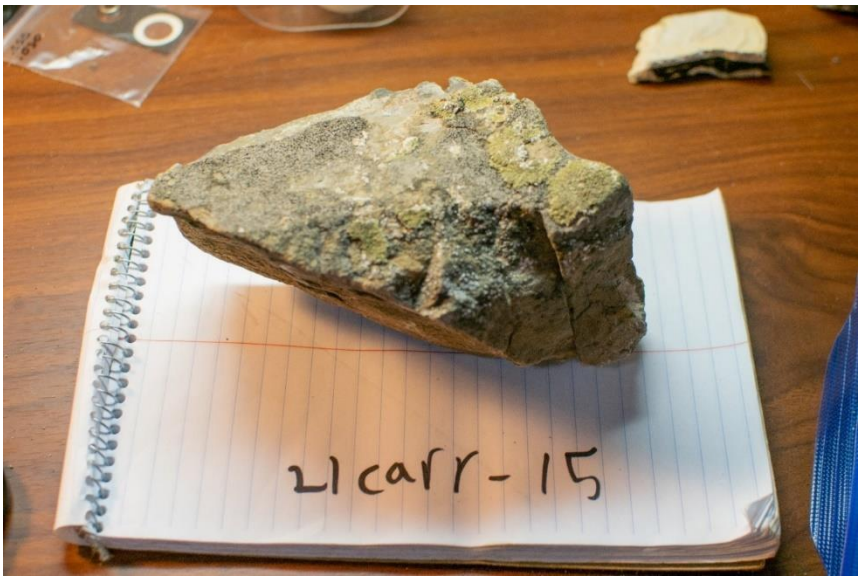

Figure 32. Sample 15 hand sample photo.

Sample 11

Sample 11 is a phaneritic, hypidiomorphic, medium grained, light grey granodiorite sample. This sample has large tourmaline crystals present in hand that are about 1-2 centimeters in length, and with large quartz and feldspar crystals present that are about 0.5 to 1 centimeter in length.

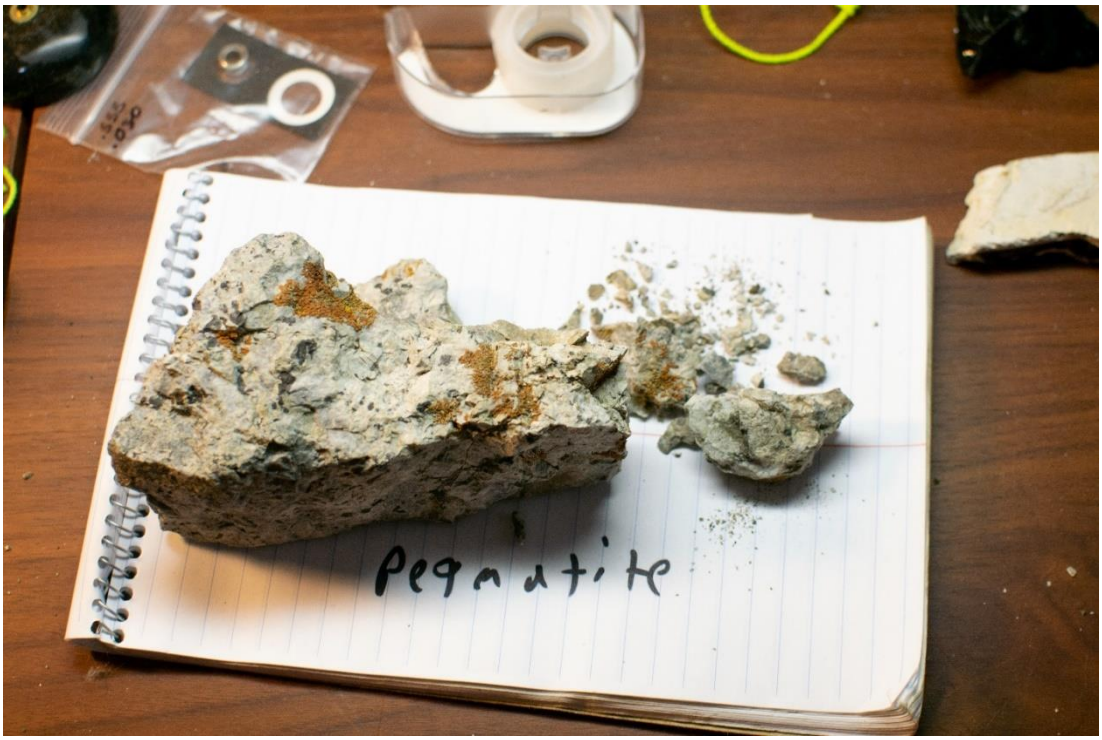

Figure 33. sample 11 hand sample photo.

II. Analyses of standard BHVO-2 showing uncertainty of XRF analysis

	Specimen	SiO_2	TiO_2	Al_2O_3	Fe_2O_3T	MnO	MgO	CaO	Na_2O	K_2O	P_2O_5	Total
	BHVO-2 A	49.693	2.716	13.33	12.64	0.169	7.104	11.436	2.149	0.506	0.274	100.018
	BHVO-2 B	50.09	2.724	13.464	12.427	0.168	7.173	11.469	2.165	0.508	0.274	100.461
	BHVO-2 B1	50.223	2.718	13.539	12.412	0.167	7.182	11.45	2.185	0.509	0.275	100.66
	BHVO-2 C	49.844	2.715	13.372	12.576	0.168	7.101	11.445	2.153	0.505	0.275	100.153
	BHVO-2 D	50.118	2.692	13.583	12.435	0.168	7.144	11.344	2.226	0.514	0.282	100.506
	BHVO-2 D1	50.111	2.689	13.597	12.442	0.168	7.145	11.338	2.224	0.513	0.281	100.509
	BHVO-2 E	49.972	2.719	13.414	12.392	0.168	7.136	11.466	2.154	0.506	0.275	100.202
	BHVO-2 F	49.873	2.706	13.414	12.55	0.166	7.136	11.405	2.157	0.505	0.275	100.187
	BHVO-2 F1	49.806	2.704	13.388	12.546	0.167	7.125	11.395	2.162	0.507	0.273	100.073
	BHVO-2 G	49.781	2.707	13.394	12.413	0.167	7.147	11.394	2.158	0.504	0.274	99.937
	BHVO-2 H	49.729	2.716	13.317	12.452	0.167	7.105	11.429	2.148	0.509	0.276	99.848
	BHVO-2 H1	49.742	2.715	13.329	12.457	0.167	7.094	11.432	2.142	0.508	0.277	99.863
	BHVO-2 I	49.863	2.71	13.39	12.406	0.167	7.147	11.439	2.163	0.505	0.275	100.064
	BHVO-2 J	49.388	2.703	13.267	12.208	0.166	7.044	11.38	2.122	0.502	0.271	99.051
	BHVO-2 J1	49.385	2.706	13.248	12.211	0.167	7.04	11.377	2.122	0.503	0.271	99.031
	BHVO-2 K	49.759	2.704	13.358	12.525	0.167	7.114	11.402	2.149	0.506	0.274	99.958
	BHVO-2 L	49.741	2.717	13.31	12.236	0.167	7.096	11.441	2.127	0.502	0.275	99.613
	BHVO-2 L1	49.73	2.718	13.336	12.236	0.167	7.104	11.442	2.134	0.502	0.274	99.642
	BHVO-2 L2	49.927	2.718	13.434	12.234	0.168	7.114	11.442	2.155	0.504	0.274	99.97
	BHVO-2 M	50.011	2.72	13.439	12.458	0.167	7.161	11.446	2.142	0.505	0.276	100.324
	BHVO-2 N	49.823	2.72	13.327	12.448	0.168	7.113	11.452	2.139	0.507	0.276	99.972
	BHVO-2 N1	49.746	2.723	13.356	12.44	0.168	7.103	11.439	2.14	0.504	0.273	99.893
	BHVO-2 O	49.596	2.699	13.294	12.35	0.166	7.086	11.359	2.143	0.504	0.273	99.469
	BHVO-2 P	50.036	2.72	13.464	12.174	0.168	7.166	11.459	2.158	0.505	0.274	100.124
	BHVO-2 P1	50.067	2.717	13.464	12.169	0.168	7.159	11.444	2.157	0.504	0.275	100.124
	BHVO-2 Q	49.58	2.712	13.31	12.534	0.167	7.082	11.426	2.123	0.504	0.272	99.71
	BHVO-2 R	49.832	2.705	13.393	12.627	0.167	7.124	11.412	2.149	0.508	0.273	100.191
	BHVO-2 R1	49.782	2.706	13.386	12.623	0.167	7.113	11.401	2.153	0.505	0.274	100.11
	BHVO-2 S	49.511	2.709	13.294	12.619	0.167	7.062	11.397	2.123	0.504	0.273	99.659
	BHVO-2 T	49.967	2.714	13.449	12.553	0.167	7.161	11.433	2.184	0.51	0.276	100.415
Mean		49.824	2.711	13.389	12.426	0.167	7.1194	11.420	2.154	0.506	0.275	99.991
Standard Dev.		0.208	0.009	0.086	0.143	0.001	0.0361	0.035	0.025	0.003	0.002	0.384
LOD - t value 2.462 (+/-)	**98% Conf. Level**	0.511	0.021	0.213	0.353	0.002	0.0889	0.086	0.062	0.007	0.006	0.947
		0.208	0.009	0.086	0.143	0.001	0.036	0.035	0.025	0.003	0.002	0.384
USGS Rec. Values		49.9	2.73	13.5	12.3	0.17	7.23	11.4	2.22	0.52	0.27	
Mean % Recovery		99.85%	99.32%	99.18%	101.03%	98.41%	98.47%	100.17%	97.01%	97.29%	101.73%	
% uncerainty		0.417	0.322	0.645	1.154	0.420	0.507	0.305	1.166	0.582	0.852	0.385

Table 3. all oxides are in weight %, LOI stands for loss of ignition, and t-values are the product of a t-test which compares a single sample mean to a population mean.

III. Repeat analysis of trace element composition of standard showing uncertainty of trace element analysis (Franklin and Marshall College)

Specimen	F30/1 (ppm)	F30/2 (ppm)	F30/3 (ppm)	F30/4 (ppm)	F30/5 (ppm)	F30/6 (ppm)	F30/7 (ppm)	F30/8 (ppm)	average	2 stdev	2 RSD (%)	% uncertainty
Rb	6.2	6	5.9	6.5	6	5.9	6.2	6.2	6.1	0.4	6.6	6.6
Sr	297	296	297	299	295	295	298	293	296.3	3.8	1.3	1.3
Y	27.2	27.4	28	27.3	27.8	28.1	27.4	27.9	27.6	0.7	2.5	2.5
Zr	135	136	134	135	134	135	134	134	134.6	1.5	1.1	1.1
V	307	310	307	313	314	310	315	304	310.0	7.7	2.5	2.5
Ni	243	245	243	243	243	243	246	245	243.9	2.5	1.0	1.0
Cr	633	671	650	669	635	638	657	665	652.3	31.1	4.8	4.8
Nb	10.8	11.2	11.8	12.2	11.7	11.2	11.6	11.3	11.5	0.9	7.6	7.6
Ga	16.2	16.3	16.5	16.5	16.4	16.6	16.5	16.4	16.4	0.3	1.6	1.6
Cu	133	132	133	133	132	132	132	133	132.5	1.1	0.8	0.8
Zn	106	106	105	105	105	106	106	106	105.6	1.0	1.0	1.0
Co	57	58	57	58	57	58	59	59	57.9	1.7	2.9	2.9
Ba	89	101	96	109	76	89	81	91	91.5	21.1	23.1	23.1
La	14	14	15	16	16	15	15	16	15.1	1.7	11.0	11.0
Ce	29	31	30	27	32	29	30	31	29.9	3.1	10.4	10.4
U	<0.5	0.9	1.1	1.7	<0.5	0.5	0.7	2	1.2	1.2	101.9	101.9
Th	3	<0.5	2.2	<0.5	1.8	2	0.9	1.4	1.9	1.4	76.1	76.1
Sc	34	33	33	34	34	33	34	33	33.5	1.1	3.2	3.2
Pb	<1	<1	<1	<1	2	3	1	2	2.0	1.6	81.6	81.6

Table 4. All the units are reported in ppm.

IV. XRF and major trace-element composition of samples.

Specimen	*Sample 4*	*Sample 9*	*Sample 10*	*Sample 11*	*Sample 14*	*Sample 15*
SiO2	41.72	40.77	39.08	38.84	42.22	45.42
TiO2	0.12	0.51	0.85	0.46	0.47	0.57
Al2O3	9.89	7.83	9.39	7.90	8.66	10.23
Fe2O3T	2.08	2.66	3.16	2.57	2.89	3.13
MnO	0.10	0.04	0.03	0.05	0.04	0.04
MgO	11.59	2.09	4.50	1.95	3.31	2.97
CaO	33.87	45.73	42.59	45.63	39.20	33.85
Na2O	0.00	0.00	0.00	0.28	0.51	0.61
K2O	0.19	0.07	0.18	1.93	2.49	2.90
P2O5	0.01	0.07	0.06	0.05	0.04	0.04
Total	**99.57**	**99.76**	**99.83**	**99.66**	**99.83**	**99.76**
LOI	10.35	11.96	13.92	14.72	18.70	17.05
Rb	2.5	5.5	4.0	75.5	94.5	112.0
Sr	257	325	138	1196	820	711
Y	2.4	19.8	66.6	17.8	17.9	21.2
Zr	19	118	163	131	122	130
V	18	46	20	62	89	102
Ni	16	14	21	19	18	21
Cr	70	54	100	87	71	70
Nb	3.3	6.9	1.6	19.4	14.0	15.0
Ga	7.0	4.9	9.9	7.0	8.3	10.2
Cu	4	12	33	15	13	11
Zn	257	25	74	46	89	78
Co	7	4	3	4	9	6
Ba	22	41	11	599	235	303
La	<2	40	4	13	18	23
Ce	5	77	22	<2	28	32
U	0.9	2.9	2.2	1.2	0.9	2.2
Th	2.6	3.8	1.6	4.8	6.6	6.9
Sc	23	43	42	44	36	34
Pb	15	3	2	5	20	9

Table 5. All oxides are in weight % and trace elements are in ppm.

V. Recorded isotope values for the samples. averages, and standard deviations

Sample	*mass_mg*	*δ¹³C‰*	*δ¹⁸O‰*	***triplicate estimates***		
				δ¹³C	δ¹⁸O	
Sample 14	0.109	4.345070579	23.56245719			
Sample 14	0.245	4.497989705	23.47204355	**4.431598**	**23.53821**	**mean**
Sample 14	0.269	4.451734045	23.58013785	**0.078423**	**0.057982**	**std**
Sample 13	10.8	-5.144511092	17.47551186			
Sample 13	9.566	-5.461731259	17.37367008	**-5.45723**	**17.30275**	**mean**
Sample 13	10.575	-5.765460062	17.05906756	**0.310499**	**0.217092**	**std**
Sample 15	0.122	3.992277748	22.11363407			
Sample 15	0.319	4.120680311	22.08726369	**4.039281**	**22.08784**	**mean**
Sample 15	0.308	4.004886372	22.06262674	**0.070775**	**0.025509**	**std**
Sample 4	0.701	-6.513545854	14.79649271			
Sample 4	1.306	-5.711246091	14.52590569	**-6.05768**	**14.74476**	**mean**
Sample 4	0.915	-6.031528453	14.65181348	**0.33439**	**0.205629**	**std**
Sample 4	0.958	-5.974401817	15.00483161			
Sample 8	0.138	-0.830871035	17.47574018			
Sample 8	0.444	-0.820023922	17.0730777	**-0.84603**	**17.36128**	**mean**
Sample 8	0.435	-0.865291043	17.40852322	**0.024199**	**0.195274**	**std**
Sample 8	0.4	-0.867930188	17.48778143			
Sample 9	0.736	-7.278446741	16.78024376			
Sample 9	0.542	-7.112646267	16.78959664	**-7.17685**	**16.82636**	**mean**
Sample 9	0.56	-7.139449235	16.90924463	**0.089002**	**0.071931**	**std**
Sample 10	0.313	-10.57658639	17.9153895			
Sample 10	0.285	-10.69554793	17.95931091	**-10.6887**	**18.02006**	**mean**

Sample 10	0.34	-10.79383065	18.18546578	**0.108786**	**0.144923**	**std**

VI. Isotope standards MCC, and JCC standard deviations and averages.

$\delta^{13}C‰$	**$\delta^{18}O‰$**	
JTB		
1.78	21.94	**Means**
0.04	0.08	**Stds**
MCC		
-36.01	8.52	**Means**
0.031561	0.070436	**Stds**

Table 7. All oxides are in weight % and trace elements are in ppm.

VII. WDS data

Cation Total	Group : C	Sample : AB	Page	1									
No.	Na	Fe	Ti	Ca	Al	Mg	Mn	K	Si	O	Total	Comment	
1	0.0024	0.0037	0	3.992	0.0009	0.0049	0.0043	0	3.996	0	8.0042	Wo	
2	0	0.0026	0.0008	3.981	0.0032	0.0063	0.0022	0	4.001	0	7.9971	Wo	
3	0	0.0054	0	3.993	0.0009	0.0063	0.0043	0.0007	3.994	0	8.0047	Wo	
4	0.401	0.692	0.275	0.808	1.313	1.446	0.0029	0.207	3.113	0	8.2579	Hb-Kak	
5	0.392	0.698	0.266	0.794	1.32	1.464	0.0032	0.205	3.115	0	8.2572	Hb-Kak	
6	0.399	0.703	0.266	0.791	1.317	1.476	0.0044	0.209	3.107	0	8.2724	Hb-Kak	
7	0	1.335	0.71	3.208	0.54	0.093	0.0027	0.0015	2.566	0	8.4562	19-10 Isotropic Phase (Grt?) Nr Reg 3	
8	0.0026	1.417	0.716	3.073	0.542	0.092	0.0012	0.0009	2.585	0	8.4297	19-10 Isotropic Phase (Grt?) Nr Reg 3	
9	0.0019	1.337	0.603	3.133	0.605	0.1002	0.0011	0	2.657	0	8.4382	19-10 Isotropic Phase (Grt?) Nr Reg 3	
10	0.0042	0.232	0.0541	3.084	1.515	0.432	0.0008	0.0017	2.933	0	8.2568	19-10 Ves Nr Reg 3	
11	0.0052	0.065	0.0083	3.777	0.4	0.1245	0	0.0008	3.707	0	8.0878	19-10 Ves Nr Reg 3	
12	0.0017	0.231	0.0776	3.096	1.493	0.419	0	0.0006	2.929	0	8.2479	19-10 Ves Nr Reg 3	
13	0.0064	0.0015	0	11.988	0	0.006	0	0.001	0	0	12.0029	19-10 Cc vein Nr Reg 3	
14	0.002	0.006	0	11.958	0.0052	0.0202	0	0.0048	0.0024	0	11.9987	19-10 Cc vein Nr Reg 4	
15	0	0.0047	0	11.963	0	0.0166	0	0.0042	0.0067	0	11.9952	19-10 Cc vein Nr Reg 5	
16	0.001	0.0036	0.0034	3.95	0.0135	0.0099	0.0014	0	4.004	0	7.9869	19-10 Calc-Silicate Nr Reg 1 (fibrous)	wollastonite
17	0.0074	0.0033	0.0044	4.005	0.0145	0.0122	0	0.0017	3.972	0	8.0205	19-10 Calc-Silicate Nr Reg 1 (fibrous)	wollastonite
18	0.001	0.0051	0.0032	4.027	0.0116	0.0202	0.0032	0.0008	3.96	0	8.0322	19-10 Calc-Silicate Nr Reg 1 (fibrous)	wollastonite
19	0.0145	0.0006	0	2.294	0.0276	0	0	0.438	4.719	0	7.4938	19-10 Ca-Si-K Nr Reg 1 Dark in BSE	
20	0.0217	0.0064	0	2.335	0.0315	0	0.0023	0.43	4.692	0	7.5189	19-10 Ca-Si-K Nr Reg 1 Dark in BSE	
21	0.0084	0.0011	0	2.354	0.0116	0	0	0.47	4.694	0	7.5391	19-10 Ca-Si-K Nr Reg 1 Dark in BSE	
22	0	1.374	0.7	3.205	0.553	0.102	0.0031	0	2.543	0	8.4801	19-10 Ca-Si-Fe-Ti-Al Nr Reg 1 lt in BSE	
23	0	1.423	0.705	3.17	0.52	0.0984	0.0007	0	2.558	0	8.4752	19-10 Ca-Si-Fe-Ti-Al Nr Reg 1 lt in BSE	
24	0.0083	1.247	0.548	3.154	0.651	0.1064	0	0	2.708	0	8.4227	19-10 Ca-Si-Fe-Ti-Al Nr Reg 1 lt in BSE	
25	0	0.0047	0.0032	3.979	0.0173	0.0103	0	0.0008	3.987	0	8.0023	19-10 Equant Phase Nr Reg 1 int in BSE	Wollastonite
26	0	0.004	0.0064	4.052	0.0187	0.01	0	0	3.947	0	8.0381	19-10 Equant Phase Nr Reg 1 int in BSE	Wollastonite
27	0.0022	0.0044	0.0057	3.98	0.0196	0.0089	0.0015	0.0012	3.982	0	8.0056	19-10 Equant Phase Nr Reg 1 int in BSE	Wollastonite
28	0.0258	0.217	0.103	3.034	1.597	0.251	0.0048	0.0006	2.939	0	8.1722	19-8 Near Region 1 (Elongate) Ves?	
29	0.0216	0.232	0.0858	3.059	1.634	0.226	0.0022	0	2.924	0	8.1846	19-8 Near Region 1 (Elongate) Ves?	
30	0.0094	0.214	0.11	3.084	1.536	0.28	0.0025	0	2.945	0	8.181	19-8 Near Region 1 (Elongate) Ves?	
31	0.003	0.001	0.0019	11.956	0.0052	0.0114	0	0.0276	0.0025	0	12.0087	19-8 Near Region 1 (Cc)	
32	0	0.0044	0	11.981	0.001	0.0104	0	0.0054	0	0	12.0022	19-8 Near Region 1 (Cc)	
33	0	0.0014	0.0087	11.98	0	0	0	0.003	0	0	11.9931	19-8 Near Region 1 (Cc)	

Brodsky 40

Cation To Group Sample : Page 1												
No.	Na	Fe	Ti	Ca	Al	Mg	Mn	K	Si	O	Total	Comment
34	0.0057	0.125	0.0054	0.0028	1.537	2.965	0.005	1.057	3.027	0	8.7299	19-9 Region 1 Sheet Silicate
35	0.0069	0.127	0.0055	0.0087	1.49	3.004	0.0024	1.049	3.042	0	8.7355	19-9 Region 1 Sheet Silicate
36	0.003	0.128	0.003	0.0166	1.482	2.993	0.0026	1.02	3.059	0	8.7072	19-9 Region 1 Sheet Silicate
37	0	0.671	0.0696	3.061	1.333	0.0471	0.0032	0.0011	3.04	0	8.226	19-9 Region 7 High BSE Equant
38	0.0049	0.463	0.125	3.032	1.475	0.084	0.0041	0.0036	2.976	0	8.1677	19-9 Region 7 High BSE Equant
39	0.001	0.71	0.0905	3.056	1.3	0.0477	0.0028	0.0042	3.025	0	8.2372	19-9 Region 7 High BSE Equant
40	0	0.0071	0.0042	11.972	0.0031	0	0.0019	0.0125	0	0	12.0008	19-9 Region 7 Cc
41	0	0.0021	0	11.989	0.0032	0.0038	0	0	0	0	11.9981	19-9 Region 7 Cc
42	0	0.0039	0	11.994	0.001	0	0	0.001	0	0	12	19-9 Region 7 Cc
43	0.0024	0.19	0.0247	3.103	1.575	0.49	0.0057	0	2.899	0	8.2898	19-9 Region 2.1
44	0.0014	0.293	0.0596	3.08	1.533	0.377	0.0018	0.0009	2.914	0	8.2607	19-9 Region 2.1
45	0.0025	0.305	0.0664	3.054	1.539	0.395	0.0013	0.0015	2.901	0	8.2657	19-9 Region 2.1
46	0.0019	0.281	0.0688	3.021	1.453	0.395	0.0012	0	2.992	0	8.2139	19-9 Region 2.1
47	0	0.295	0.0731	3.093	1.524	0.391	0.0016	0.001	2.893	0	8.2717	19-9 Region 2.1
48	0.0012	0.293	0.0581	3.077	1.492	0.418	0.0029	0.0012	2.927	0	8.2705	19-9 Region 2.1
49	0.001	0.206	0.0288	3.042	1.571	0.472	0.0016	0	2.932	0	8.2544	19-9 Region 10
50	0	0.215	0.0316	3.086	1.554	0.439	0.0016	0.0023	2.931	0	8.2605	19-9 Region 10
51	0.0029	0.203	0.0268	3.078	1.566	0.469	0.002	0	2.922	0	8.2697	19-9 Region 10
52	0.0019	0.164	0.0078	3.093	1.622	0.459	0.0012	0	2.917	0	8.266	18-4 Region 1
53	0	0.173	0.0077	3.057	1.584	0.47	0.0016	0	2.953	0	8.2463	18-4 Region 2
54	0.001	0.166	0.0009	3.091	1.632	0.454	0	0	2.919	0	8.2639	18-4 Region 3
55	0	0.0006	0	4.017	0.0129	0.0052	0.0026	0	3.978	0	8.0163	18-4 Region (2)
56	0	0	0	4.005	0.0129	0.0026	0	0	3.987	0	8.0075	18-4 Region (2)
57	0	0.0017	0	3.992	0.0147	0.0028	0	0.0014	3.99	0	8.0026	18-4 Region (2)
58	0.0013	0.14	0	0.0399	0.005	3.982	0.0271	0.0021	3.901	0	8.0984	18-4 Region (3ish) Mg<Si (EDS)
59	0.0022	0.14	0	0.0433	0.0041	3.929	0.0286	0	3.926	0	8.0732	18-4 Region (3ish) Mg<Si (EDS)
60	0.0013	0.138	0.0006	0.0455	0.0038	3.894	0.0308	0.0014	3.942	0	8.0574	18-4 Region (3ish) Mg<Si (EDS)
61	0.0113	0.0025	0	2.401	0.001	0	0.002	0.399	4.694	0	7.5108	18-4 Region (3ish) K<Ca<Si (EDS
62	0.0046	0.0027	0	2.217	0.0113	0.027	0.0011	0.1107	4.839	0	7.2134	18-4 Region (3ish) K<Ca<Si (EDS
63	0.0198	0.0016	0	2.38	0.0017	0.0012	0	0.408	4.7	0	7.5123	18-4 Region (3ish) K<Ca<Si (EDS
64	0	0.002	0	4.414	0.0021	0.0016	0.0036	0	3.788	0	8.2113	18-4 Region 5 high order biref
65	0	0.0038	0	4.419	0.0038	0	0.0058	0	3.783	0	8.2154	18-4 Region 5 high order biref
66	0.001	0.0027	0	4.407	0.0038	0	0.0135	0	3.785	0	8.213	18-4 Region 5 high order biref

Orange= wollastonite
white= Serpentine- group minerals
Green= Vesuvianite
Grey= serpentine group minerals
Red= Grossular-andradite
Bright blue= scawtite
Yellow= andradite-schorlomite-grossular garnet
Light blue= Calcite
Brown = Phlogopite

VIII. EDS spectra for minerals

Calcite

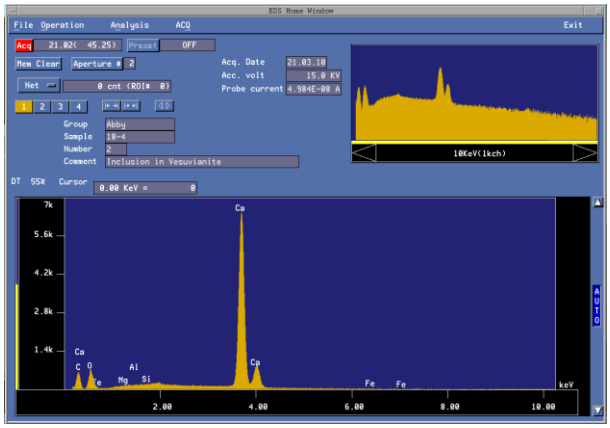

Wollastonite

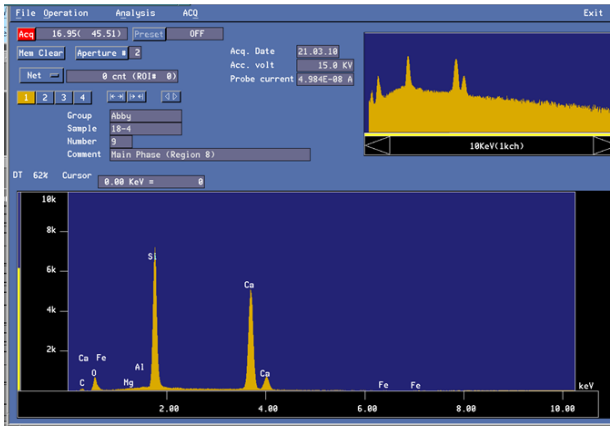

Phlogopite

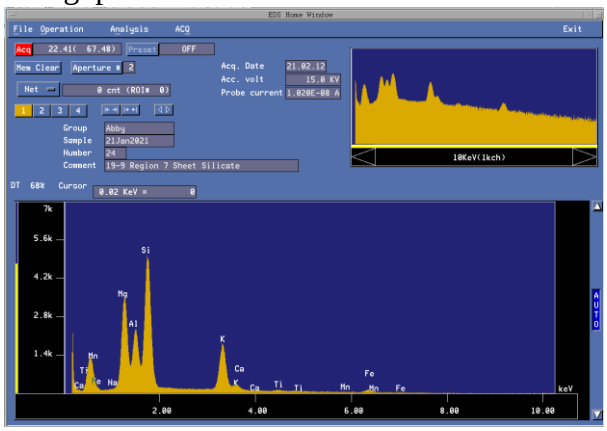

Grossular-andradite garnet

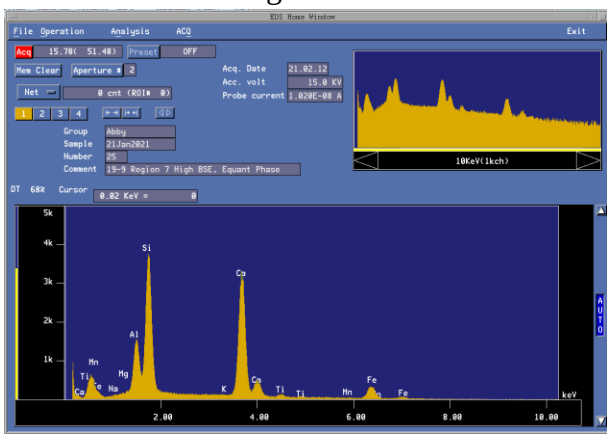

Vesuvianite

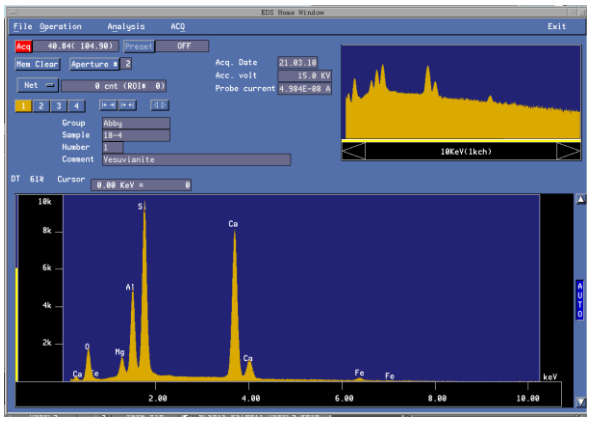

Scawtite

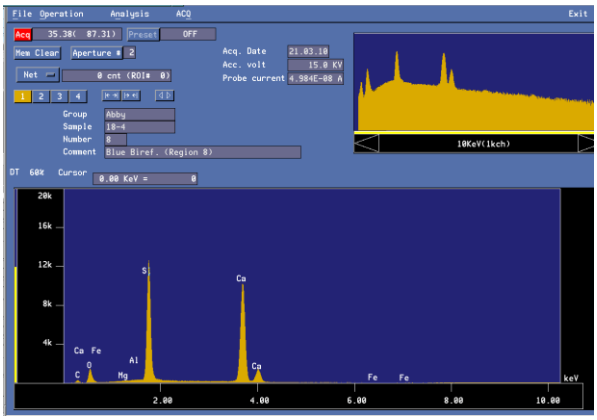

Serpentine

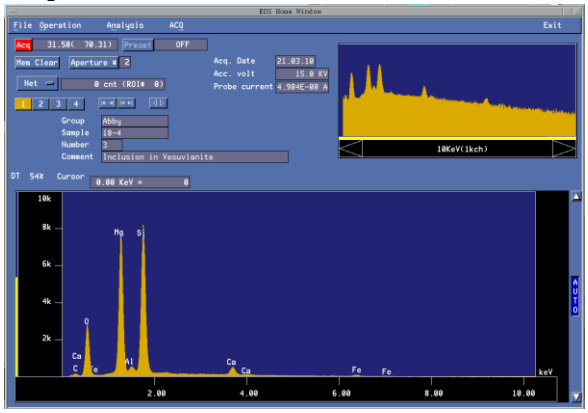

Andradite-schorlomite-grossular garnet

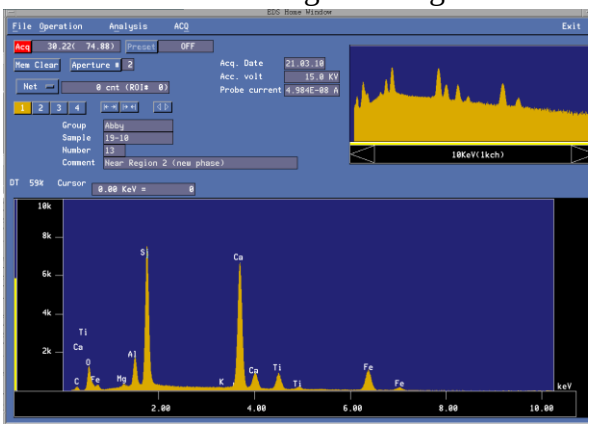

IX. Limestone variability

Specimen	21-14	21-15	Average	Standard Deviation	Log (C'/C_0)
SiO2	42.22	45.42	43.82	1.6	-0.03173
TiO2	0.47	0.57	0.52	0.05	-0.08378
Al2O3	8.66	10.23	9.45	0.785	-0.07236
Fe2O3T	2.89	3.13	3.01	0.12	-0.03465
MnO	0.04	0.04	0.04	0	0
MgO	3.31	2.97	3.14	0.17	0.047072
CaO	39.20	33.85	36.53	2.6755	0.063738
Na2O	0.51	0.61	0.56	0.05	-0.07776
K2O	2.49	2.90	2.70	0.205	-0.0662
P2O5	0.04	0.04	0.04	0	0
Total	99.83	99.76	99.80	0.0355	
LOI	18.70	17.05	17.88	0.825	
Rb	94.50	112.00	103.25	8.75	-0.07379
Sr	820.00	711.00	765.50	54.5	0.061944
Y	17.90	21.20	19.55	1.65	-0.07348
Zr	122.00	130.00	126.00	4	-0.02758
V	89.00	102.00	95.50	6.5	-0.05921
Ni	18.00	21.00	19.50	1.5	-0.06695
Cr	71.00	70.00	70.50	0.5	0.00616
Nb	14.00	15.00	14.50	0.5	-0.02996
Ga	8.30	10.20	9.25	0.95	-0.08952
Cu	13.00	11.00	12.00	1	0.072551
Zn	89.00	78.00	83.50	5.5	0.057295
Co	9.00	6.00	7.50	1.5	0.176091
Ba	235.00	303.00	269.00	34	-0.11037
La	18.00	23.00	20.50	2.5	-0.10646
Ce	28.00	32.00	30.00	2	-0.05799
U	0.90	2.20	1.55	0.65	-0.38818
Th	6.60	6.90	6.75	0.15	-0.01931
Sc	36.00	34.00	35.00	1	0.024824
Pb	20.00	9.00	14.50	5.5	0.346787

Table 9. All oxides are in weight % and trace elements are in ppm.

X. Immobile reference frame analysis

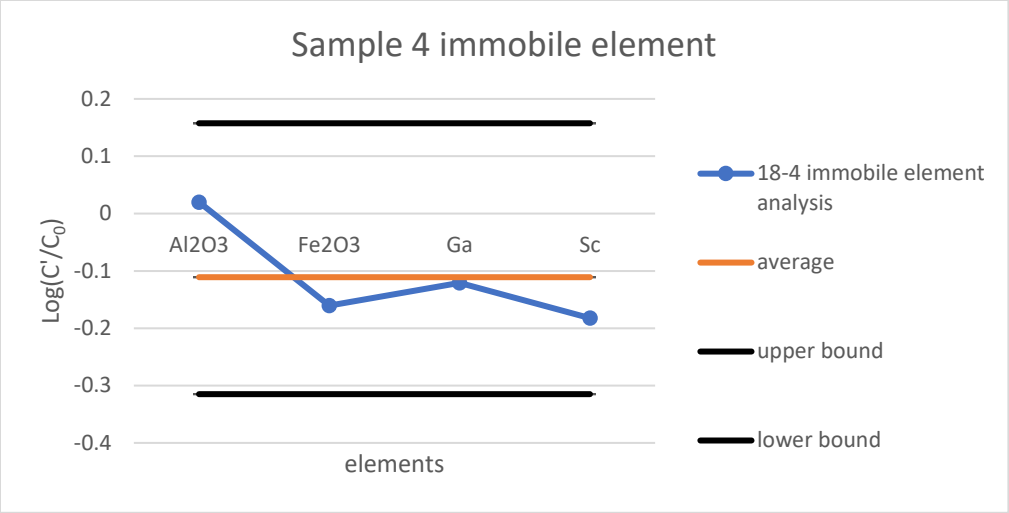

Figure 33. A graph of sample 4 immobile element analysis.

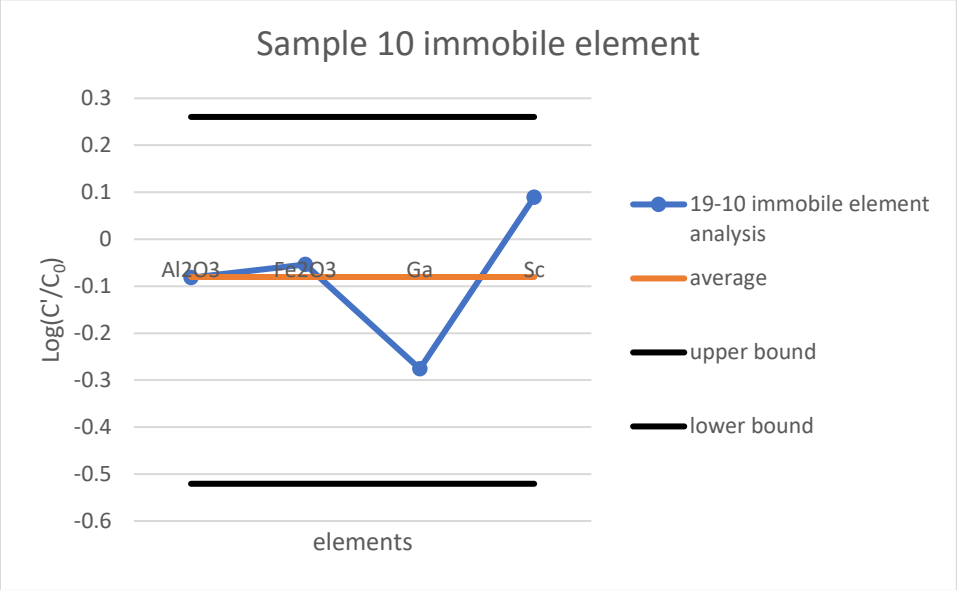

Figure 34. A graph of sample 10 immobile element analysis.

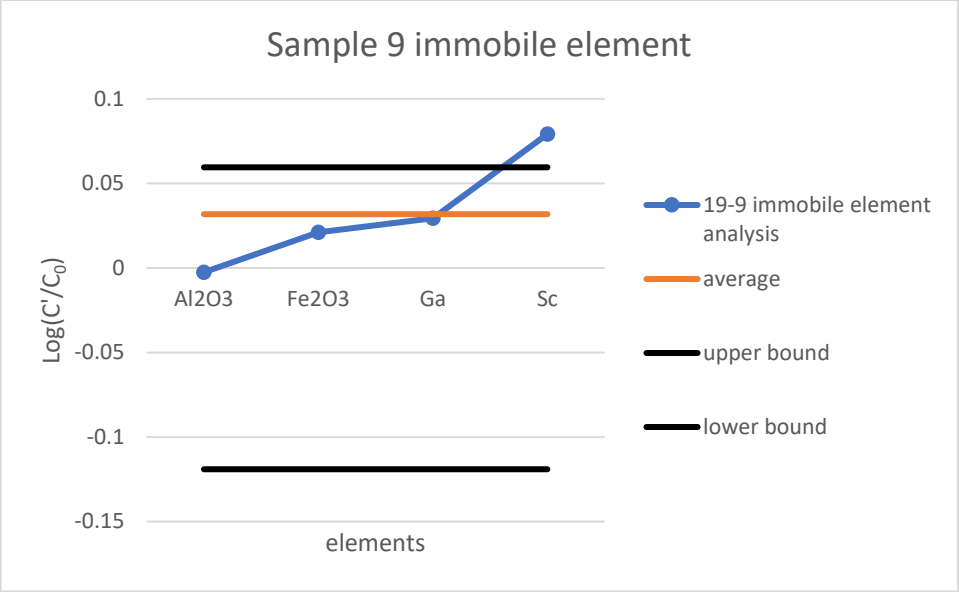

Figure 35. A graph of sample 9 immobile element analysis.

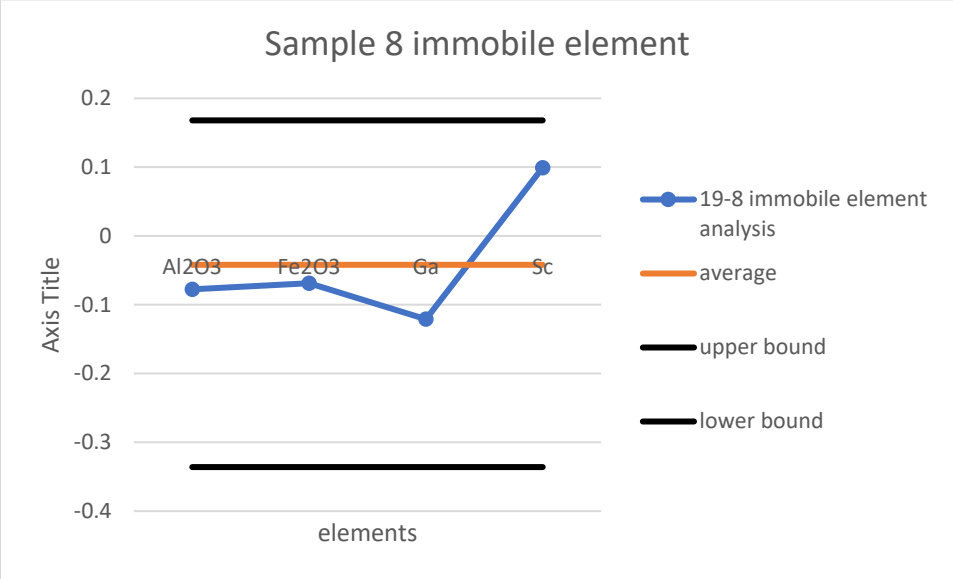

Figure 36. A graph of the sample 8 immobile element analysis.

XI. Perple_X pseudosections

All the pseudosections in this section only display 1 to 3 of the minerals present in each sample and include many minerals that were not observed in any of the samples.

Abbreviation key for Perple_X	
gr	Grossular
di	Diopside

an	Anorthite
kals	Kalsilite
ilm	Ilmenite
herc	Hercynite
phl	Phlogophite
clin	clinochlore(ordered)
q	Quartz
sph	Titanite
sp	Spinel
san	Sanidine
lc	Leucite
vsv	Vesuvianite
fa	Fayalite
Gt(W)	garnet created from the White (2014) phase solution model.
dol	Dolomite
Wo	Wollastonite
hed	Hedenbergite

Sample 19-9 pseudosection

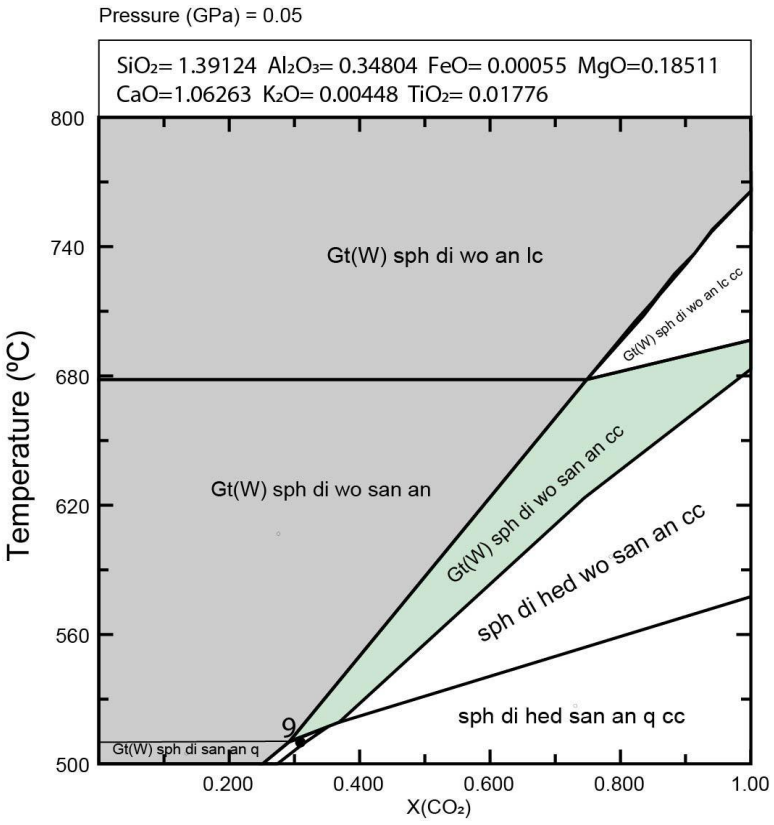

Figure 37. Sample 9's pseudosection Gt(W) refers to a garnet phase solution model from White, 2014. The light green represents the closest matching field to the sample.

Sample 18-4 pseudosection

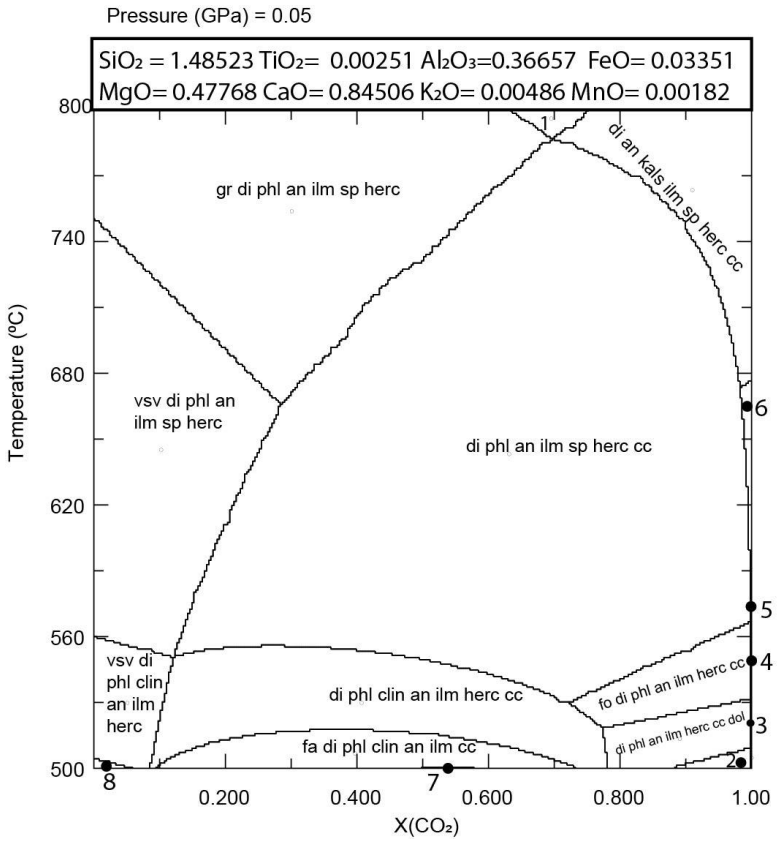

Figure 38. sample 4's pseudosection, any of the fields with vesuvianite are the closest match to the rock.

Numbered phases for Perple_X pseudosections	
1	gr di an kals ilm sp herc
2	fa di san an ilm cc di
3	di san an ilm herc cc
4	fo di san an ilm herc
5	di san an ilm sp herc
6	di an lc ilm sp herc cc
7	di phl clin an ilm cc acti
8	fa vsv di phl clin an ilm
9	Gt(W) sph di san an q cc

XII. Academic integrity statement "I pledge on my honor that I have not given or received any unauthorized assistance or plagiarized on this assignment."